Ultrasound-Responsive Cavitation Nuclei for Therapy and Drug Delivery

Kooiman, Klazina; Roovers, Silke; Langeveld, Simone A.G.; Kleven, Robert T.; Dewitte, Heleen; O'Reilly, Meaghan A.; Escoffre, Jean Michel; Bouakaz, Ayache; Verweij, Martin D.; More Authors

DOI
10.1016/j.ultrasmedbio.2020.01.002

Publication date
2020

Document Version
Final published version

Published in
Ultrasound in Medicine and Biology

Ultrasound in Med. & Biol., Vol. 46, No. 6, pp. 1296–1325, 2020

0301-5629/$ - see front matter

https://doi.org/10.1016/j.ultrasmedbio.2020.01.002

● *Review*

ULTRASOUND-RESPONSIVE CAVITATION NUCLEI FOR THERAPY AND DRUG DELIVERY

Klazina Kooiman,[*] Silke Roovers,[†] Simone A.G. Langeveld,[*] Robert T. Kleven,[‡] Heleen Dewitte,[†,§,¶] Meaghan A. O'Reilly,[‖,#] Jean-Michel Escoffre,[**] Ayache Bouakaz,[**] Martin D. Verweij,[*,††] Kullervo Hynynen,[‖,#,‡‡] Ine Lentacker,[†,¶] Eleanor Stride,[§§] and Christy K. Holland[‡,¶¶]

[*] Department of Biomedical Engineering, Thoraxcenter, Erasmus MC University Medical Center Rotterdam, Rotterdam, The Netherlands; [†] Ghent Research Group on Nanomedicines, Lab for General Biochemistry and Physical Pharmacy, Department of Pharmaceutical Sciences, Ghent University, Ghent, Belgium; [‡] Department of Biomedical Engineering, College of Engineering and Applied Sciences, University of Cincinnati, Cincinnati, OH, USA; [§] Laboratory for Molecular and Cellular Therapy, Medical School of the Vrije Universiteit Brussel, Jette, Belgium; [¶] Cancer Research Institute Ghent (CRIG), Ghent University Hospital, Ghent University, Ghent, Belgium; [‖] Physical Sciences Platform, Sunnybrook Research Institute, Toronto, Ontario, Canada; [#] Department of Medical Biophysics, University of Toronto, Toronto, Ontario, Canada; [**] UMR 1253, iBrain, Université de Tours, Inserm, Tours, France; [††] Laboratory of Acoustical Wavefield Imaging, Faculty of Applied Sciences, Delft University of Technology, Delft, The Netherlands; [‡‡] Institute of Biomaterials and Biomedical Engineering, University of Toronto, Toronto, Canada; [§§] Institute of Biomedical Engineering, Department of Engineering Science, University of Oxford, Oxford, United Kingdom; and [¶¶] Department of Internal Medicine, Division of Cardiovascular Health and Disease, University of Cincinnati, Cincinnati, OH, USA

(*Received* 2 *October* 2019; *revised* 20 *December* 2019; *in final from* 7 *January* 2020)

Abstract—Therapeutic ultrasound strategies that harness the mechanical activity of cavitation nuclei for beneficial tissue bio-effects are actively under development. The mechanical oscillations of circulating microbubbles, the most widely investigated cavitation nuclei, which may also encapsulate or shield a therapeutic agent in the bloodstream, trigger and promote localized uptake. Oscillating microbubbles can create stresses either on nearby tissue or in surrounding fluid to enhance drug penetration and efficacy in the brain, spinal cord, vasculature, immune system, biofilm or tumors. This review summarizes recent investigations that have elucidated interactions of ultrasound and cavitation nuclei with cells, the treatment of tumors, immunotherapy, the blood–brain and blood–spinal cord barriers, sonothrombolysis, cardiovascular drug delivery and sonobactericide. In particular, an overview of salient ultrasound features, drug delivery vehicles, therapeutic transport routes and pre-clinical and clinical studies is provided. Successful implementation of ultrasound and cavitation nuclei-mediated drug delivery has the potential to change the way drugs are administered systemically, resulting in more effective therapeutics and less-invasive treatments. (E-mail: k.kooiman@erasmusmc.nl)

Key Words: **Ultrasound, Cavitation nuclei, Therapy, Drug delivery, Bubble–cell interaction, Sonoporation, Sonothrombolysis, Blood–brain barrier opening, Sonobactericide, Tumor.**

INTRODUCTION

Around the start of the European Symposium on Ultrasound Contrast Agents, ultrasound-responsive cavitation nuclei were reported to have therapeutic potential. Thrombolysis was reported to be accelerated *in vitro* (Tachibana and Tachibana 1995), and cultured cells were transfected with plasmid DNA (Bao et al. 1997). Since then, many research groups have investigated the use of cavitation nuclei for multiple forms of therapy, including tissue ablation and drug and gene delivery. In the early years, the most widely investigated cavitation nuclei were gas microbubbles, ~1–10 μm in diameter and coated with a stabilizing shell, whereas today both solid and liquid nuclei, which can be as small as a few hundred nanometers, are also being investigated. Drugs can be co-administered with the cavitation nuclei or

Address correspondence to: Klazina Kooiman, Office Ee2302, PO Box 2040, 3000 CA Rotterdam, The Netherlands. E-mail: k.kooiman@erasmusmc.nl

loaded in or on them (Lentacker et al. 2009; Kooiman et al. 2014). The diseases that can be treated with ultrasound-responsive cavitation nuclei include but are not limited to cardiovascular disease and cancer (Sutton et al. 2013; Paefgen et al. 2015), the current leading causes of death worldwide according to the World Health Organization (Nowbar et al. 2019). This review focuses on the latest insights into cavitation nuclei for therapy and drug delivery from the physical and biological mechanisms of bubble−cell interaction to pre-clinical (both *in vitro* and *in vivo*) and clinical (time span: 2014-2019) studies, with particular emphasis on the key clinical applications. The applications covered in this review are the treatment of tumors, immunotherapy, blood−brain barrier (BBB) and blood−spinal cord barrier, dissolution of clots, cardiovascular drug delivery and treatment of bacterial infections.

CAVITATION NUCLEI FOR THERAPY

The most widely used cavitation nuclei are phospholipid-coated microbubbles with a gas core. For the 128 pre-clinical studies included in the treatment sections of this review, the commercially available and clinically approved Definity (Luminity in Europe; octafluoropropane gas core, phospholipid coating) (Definity 2011; Nolsøe and Lorentzen 2016) microbubbles were the most frequently used (in 22 studies). Definity was used for studies on all applications discussed here, mostly for opening the BBB (12 studies). SonoVue (Lumason in the United States) is commercially available and clinically approved as well (sulfur hexafluoride gas core, phospholipid coating) (Lumason 2016; Nolsøe and Lorentzen 2016) and was used in a total of 14 studies for treatment of non-brain tumors (*e.g.,* Xing et al. 2016), BBB opening (*e.g.,* Goutal et al. 2018) and sonobactericide (*e.g.*, Hu et al. 2018). Other commercially available microbubbles were used that are not clinically approved, such as BR38 (Schneider et al. 2011) in the study by Wang et al. (2015d) and MicroMarker (VisualSonics) in the study by Theek et al. (2016). Custom-made microbubbles are as diverse as their applications, with special characteristics tailored to enhance different therapeutic strategies. Different types of gasses were used as the core such as air (*e.g.,* Eggen et al. 2014), nitrogen (*e.g.,* Dixon et al. 2019), oxygen (*e.g.,* Fix et al. 2018), octafluoropropane (*e.g.,* Pandit et al. 2019), perfluorobutane (*e.g.,* Dewitte et al. 2015), sulfur hexafluoride (Bae et al. 2016; Horsley et al. 2019) or a mixture of gases such as nitric oxide and octafluoropropane (Sutton et al. 2014) or sulfur hexafluoride and oxygen (McEwan et al. 2015). While fluorinated gases improve the stability of phospholipid-coated microbubbles (Rossi et al. 2011), other gases can be loaded for therapeutic applications, such as oxygen for treatment of tumors (McEwan et al. 2015; Fix et al. 2018; Nesbitt et al. 2018) and nitric oxide (Kim et al. 2014; Sutton et al. 2014) and hydrogen gas (He et al. 2017) for treatment of cardiovascular disease. The main phospholipid component of custom-made microbubbles is usually a phosphatidylcholine such as 1,2-dipalmitoyl-*sn*-glycero-3-phosphocholine (DPPC), used in 13 studies (*e.g.,* Dewitte et al. 2015; Bae et al. 2016; Chen et al. 2016; Fu et al. 2019), or 1,2-distearoyl-*sn*-glycero-3-phosphocholine (DSPC), used in 18 studies (*e.g.,* Kilroy et al. 2014; Bioley et al. 2015; Dong et al. 2017; Goyal et al. 2017; Pandit et al. 2019). These phospholipids are popular because they are also the main components in Definity (Definity 2011) and SonoVue/Lumason (Lumason 2016), respectively. Another key component of the microbubble coating is a polyethylene glycol (PEG)ylated emulsifier such as polyoxyethylene (40) stearate (PEG40-stearate; *e.g.,* Kilroy et al. 2014) or the most frequently used 1,2-distearoyl-*sn*-glycero-3-phosphoethanolamine-*N*-carboxy(polyethylene glycol) (DSPE−PEG2000; *e.g.,* Belcik et al. 2017), which is added to inhibit coalescence and to increase the *in vivo* half-life (Ferrara et al. 2009). In general, two methods are used to produce custom-made microbubbles: mechanical agitation (*e.g.,* Ho et al. 2018) and probe sonication (*e.g.,* Belcik et al. 2015). Both methods produce a population of microbubbles that is polydisperse in size. Monodispersed microbubbles produced by microfluidics have recently been developed, and are starting to gain attention for pre-clinical therapeutic studies. Dixon et al. (2019) used monodisperse microbubbles to treat ischemic stroke.

Various therapeutic applications have inspired the development of novel cavitation nuclei, which is discussed in depth in the companion review by Stride et al. (2020). To improve drug delivery, therapeutics can be either co-administered with or loaded onto the microbubbles. One strategy for loading is to create microbubbles stabilized by drug-containing polymeric nanoparticles around a gas core (Snipstad et al. 2017). Another strategy is to attach therapeutic molecules or liposomes to the outside of microbubbles, for example, by biotin−avidin coupling (Dewitte et al. 2015; McEwan et al. 2016; Nesbitt et al. 2018). Echogenic liposomes can be loaded with different therapeutics or gases and have been studied for vascular drug delivery (Sutton et al. 2014), treatment of tumors (Choi et al. 2014) and sonothrombolysis (Shekhar et al. 2017). Acoustic Cluster Therapy (ACT) combines Sonazoid microbubbles with droplets that can be loaded with therapeutics for

treatment of tumors (Kotopoulis et al. 2017). The cationic microbubbles utilized in the treatment sections of this review were used mostly for vascular drug delivery, with genetic material loaded on the microbubble surface by charge coupling (*e.g.,* Cao et al. 2015). Besides phospholipids and nanoparticles, microbubbles can also be coated with denatured proteins such as albumin. Optison (Optison 2012) is a commercially available and clinically approved ultrasound contrast agent that is coated with human albumin and used in studies on treatment of non-brain tumors (Xiao et al. 2019), BBB opening (Kovacs et al. 2017b; Payne et al. 2017) and immunotherapy (Sta Maria et al. 2015). Nano-sized particles cited in this review have been used as cavitation nuclei for treatment of tumors, such as nanodroplets (*e.g.,* Cao et al. 2018) and nanocups (Myers et al. 2016); for BBB opening (nanodroplets; Wu et al. 2018); and for sonobactericide (nanodroplets; Guo et al. 2017a).

BUBBLE–CELL INTERACTION

Physics

The physics of the interaction between bubbles or droplets and cells are described as these are the main cavitation nuclei used for drug delivery and therapy.

Physics of microbubble–cell interaction. Being filled with gas and/or vapor makes bubbles highly responsive to changes in pressure, and hence, exposure to ultrasound can cause rapid and dramatic changes in their volume. These volume changes in turn give rise to an array of mechanical, thermal and chemical phenomena that can significantly influence the bubbles' immediate environment and mediate therapeutic effects. For the sake of simplicity, these phenomena are discussed in the context of a single bubble. It is important to note, however, that biological effects are typically produced by a population of bubbles and the influence of inter-bubble interactions should not be neglected.

Mechanical effects. A bubble in a liquid is subject to multiple competing influences: the driving pressure of the imposed ultrasound field; the hydrostatic pressure imposed by the surrounding liquid; the pressure of the gas and/or vapor inside the bubble; surface tension and the influence of any coating material; the inertia of the surrounding fluid; and damping caused by the viscosity of the surrounding fluid and/or coating, thermal conduction and/or acoustic radiation.

The motion of the bubble is determined primarily by the competition between the liquid inertia and the internal gas pressure. This competition can be characterized by using the Rayleigh–Plesset equation for bubble dynamics to compare the relative contributions of the terms describing inertia and pressure to the acceleration of the bubble wall (Flynn 1975a):

$$\ddot{R} = -\left(\frac{3}{2}\frac{\dot{R}^2}{R}\right) + \left(\frac{p_G(R) + p_\infty(t) - \frac{2\sigma}{R}}{\rho_L R}\right) = \mathrm{IF} + \mathrm{PF} \quad (1)$$

where R is the time-dependent bubble radius with initial value R_o, p_G is the pressure of the gas inside the bubble, p_∞ is the combined hydrostatic and time-varying pressure in the liquid, σ is the surface tension at the gas–liquid interface, ρ_L is the liquid density, IF is inertia factor and PF the pressure factor.

Flynn (1975a, 1975b) identified two scenarios: If the PF is dominant when the bubble approaches its minimum size, then the bubble will undergo sustained volume oscillations. If the inertia term is dominant (IF), then the bubble will undergo inertial collapse, similar to an empty cavity, after which it may rebound or it may disintegrate. Which of these scenarios occurs is dependent upon the bubble expansion ratio R_{max}/R_o and, hence, the bubble size and the amplitude and frequency of the applied ultrasound field.

Both inertial and non-inertial bubble oscillations can give rise to multiple phenomena that affect the bubble's immediate environment and hence are important for therapy. These include:

1. Direct impingement: Even at moderate amplitudes of oscillation, the acceleration of the bubble wall may be sufficient to impose significant forces on nearby surfaces, easily deforming fragile structures such as biological cell membranes (van Wamel et al. 2006; Kudo 2017) and blood vessel walls (Chen et al. 2011).
2. Ballistic motion: In addition to oscillating, the bubble may undergo translation as a result of the pressure gradient in the fluid generated by a propagating ultrasound wave (primary radiation force). Because of their high compressibility, bubbles may travel at significant velocities, sufficient to push them toward targets for improved local deposition of a drug (Dayton et al. 1999) or to penetrate biological tissue (Caskey et al. 2009; Bader et al. 2015; Acconcia et al. 2016).
3. Microstreaming: When a structure oscillates in a viscous fluid there will be a transfer of momentum as a result of interfacial friction. Any asymmetry in the oscillation will result in a net motion of that fluid in the immediate vicinity of the structure known as *microstreaming* (Kolb and Nyborg 1956). This motion will in turn impose shear stresses upon any nearby surfaces, as well as increase convection within the fluid. Because of the inherently non-linear nature of bubble oscillations (eqn [1]), both non-inertial

and inertial cavitation can produce significant microstreaming, resulting in fluid velocities on the order of 1 mm/s (Pereno and Stride 2018). If the bubble is close to a surface then it will also exhibit non-spherical oscillations, which increases the asymmetry and hence the microstreaming even further (Nyborg 1958; Marmottant and Hilgenfeldt 2003).

4. Microjetting: Another phenomenon associated with non-spherical bubble oscillations near a surface is the generation of a liquid jet during bubble collapse. If there is sufficient asymmetry in the acceleration of the fluid on either side of the collapsing bubble, then the more rapidly moving fluid may deform the bubble into a toroidal shape, causing a high-velocity jet to be emitted on the opposite side. Microjetting has been reported to be capable of producing pitting even in highly resilient materials such as steel (Naudé and Ellis 1961; Benjamin and Ellis 1966). However, as both the direction and velocity of the jet are determined by the elastic properties of the nearby surface, its effects in biological tissue are more difficult to predict (Kudo and Kinoshita 2014). Nevertheless, as reported by Chen et al. (2011), in many cases a bubble will be sufficiently confined that microjetting will have an impact on surrounding structures regardless of jet direction.
5. Shock waves: An inertially collapsing cavity that results in supersonic bubble wall velocities creates a significant discontinuity in the pressure in the surrounding liquid leading to the emission of a shock wave, which may impose significant stresses on nearby structures.
6. Secondary radiation force: At smaller amplitudes of oscillation, a bubble will also generate a pressure wave in the surrounding fluid. If the bubble is adjacent to a surface, interaction between this wave and its reflection from the surface leads to a pressure gradient in the liquid and a secondary radiation force on the bubble. As with microjetting, the elastic properties of the boundary will determine the phase difference between the radiated and reflected waves and, hence, whether the bubbles move toward or away from the surface. Motion toward the surface may amplify the effects of phenomena 1, 3 and 6.

Thermal effects. As described above, an oscillating microbubble will re-radiate energy from the incident ultrasound field in the form of a spherical pressure wave. In addition, the non-linear character of the microbubble oscillations will lead to the re-radiation of energy over a range of frequencies. At moderate driving pressures, the bubble spectrum will contain integer multiples (harmonics) of the driving frequency; and at higher pressures, also fractional components (sub- and ultraharmonics). In biological tissue, absorption of ultrasound increases with frequency and this non-linear behavior thus also increases the rate of heating (Hilgenfeldt et al. 2000; Holt and Roy 2001). Bubbles will also dissipate energy as a result of viscous friction in the liquid and thermal conduction from the gas core, the temperature of which increases during compression. Which mechanism is dominant depends on the size of the bubble, the driving conditions and the viscosity of the medium. Thermal damping is, however, typically negligible in biomedical applications of ultrasound as the time constant associated with heat transfer is much longer than the period of the microbubble oscillations (Prosperetti 1977).

Chemical effects. The temperature rise produced in the surrounding tissue will be negligible compared with that occurring inside the bubble, especially during inertial collapse when it may reach several thousand Kelvin (Flint and Suslick 1991). The gas pressure similarly increases significantly. Although only sustained for a very brief period, these extreme conditions can produce highly reactive chemical species, in particular reactive oxygen species (ROS), as well as the emission of electromagnetic radiation (sonoluminescence). ROS have been reported to play a significant role in multiple biological processes (Winterbourn 2008), and both ROS and sonoluminescence may affect drug activity (Rosenthal et al. 2004; Trachootham et al. 2009; Beguin et al. 2019).

Physics of droplet–cell interaction. Droplets consist of an encapsulated quantity of a volatile liquid, such as perfluorobutane (boiling point: −1.7˚C) or perfluoropentane (boiling point: 29˚C), which is in a superheated state at body temperature. Superheated state means that although the volatile liquids have a boiling point below 37˚C, these droplets remain in the liquid phase and do not exhibit spontaneous vaporization after injection. Vaporization can be achieved instead by exposure to ultrasound of significant amplitude via a process known as acoustic droplet vaporization (ADV) (Kripfgans et al. 2000). Before vaporization, the droplets are typically one order of magnitude smaller than the emerging bubbles, and the perfluorocarbon is inert and biocompatible (Biro and Blais 1987). These properties enable a range of therapeutic possibilities (Sheeran and Dayton 2012; Lea-Banks et al. 2019). For example, unlike microbubbles, small droplets may extravasate from the leaky vessels into tumor tissue because of the enhanced permeability and retention (EPR) effect (Long et al. 1978; Lammers et al. 2012; Maeda 2012), and then be turned into bubbles by ADV (Rapoport et al. 2009; Kopechek et al. 2013). Loading the droplets with a drug enables local delivery (Rapoport et al. 2009) by way of ADV. The mechanism behind this is that the emerging

bubbles give rise to similar radiation forces and microstreaming as described earlier in the Physics of the Microbubble−Cell Interaction. It should be noted that oxygen is taken up during bubble growth (Radhakrishnan et al. 2016), which could lead to hypoxia.

The physics of the droplet−cell interaction is largely governed by the ADV. In general, it has been observed that ADV is promoted by the following factors: large peak negative pressures (Kripfgans et al. 2000), usually obtained by strong focusing of the generated beam, high frequency of the emitted wave and a relatively long distance between the transducer and the droplet. Another observation that has been made with micrometer-sized droplets is that vaporization often starts at a well-defined nucleation spot near the side of the droplet where the acoustic wave impinges (Shpak et al. 2014). These facts can be explained by considering the two mechanisms that play a role in achieving a large peak negative pressure inside the droplet: acoustic focusing and non-linear ultrasound propagation (Shpak et al. 2016). In the following, lengths and sizes are related to the wavelength, that is, the distance traveled by a wave in one oscillation (*e.g.,* a 1-MHz ultrasound wave that is traveling in water with a wave speed, c, of 1500 m/s has a wavelength, w (m), of $c/f = 1500/10^6 = 0.0015$, that is, 1.5 mm.

Acoustic focusing. Because the speed of sound in perfluorocarbon liquids is significantly lower than that in water or tissue, refraction of the incident wave will occur at the interface between these fluids, and the spherical shape of the droplet will give rise to focusing. The assessment of this focusing effect is not straightforward because the traditional way of describing these phenomena with rays that propagate along straight lines (the ray approach) holds only for objects that are much larger than the applied wavelength. In the current case, the frequency of a typical ultrasound wave used for insonification is in the order of 1−5 MHz, yielding wavelengths in the order of 1500−300 μm, while a droplet will be smaller by two to four orders of magnitude. In addition, using the ray approach, the lower speed of sound in perfluorocarbon would yield a focal spot near the backside of the droplet, which is in contradiction to observations. The correct way to treat the focusing effect is to solve the full diffraction problem by decomposing the incident wave, the wave reflected by the droplet and the wave transmitted into the droplet into a series of spherical waves. For each spherical wave, the spherical reflection and transmission coefficients can be derived. Superposition of all the spherical waves yields the pressure inside the droplet. Nevertheless, when this approach is only applied to an incident wave with the frequency that is emitted by the transducer, this will lead neither to the right nucleation spot nor to sufficient negative pressure for vaporization. Nanoscale droplets may be too small to make effective use of the focusing mechanism, and ADV is therefore less dependent on the frequency.

Non-linear ultrasound propagation. High pressure amplitudes, high frequencies and long propagation distances all promote non-linear propagation of an acoustic wave (Hamilton and Blackstock 2008). In the time domain, non-linear propagation manifests as an increasing deformation of the shape of the ultrasound wave with distance traveled. In the frequency domain, this translates to increasing harmonic content, that is, frequencies that are multiples of the driving frequency. The total incident acoustic pressure $p(t)$ at the position of a nanodroplet can therefore be written as

$$p(t) = \sum_{n=1}^{\infty} a_n \cos(n\omega t + \phi_n) \tag{2}$$

where n is the number of a harmonic, a_n and ϕ_n are the amplitude and phase of this harmonic and ω is the angular frequency of the emitted wave. The wavelength of a harmonic wave is a fraction of the emitted wavelength.

The aforementioned effects are both important in the case of ADV and should therefore be combined. This implies that first the amplitudes and phases of the incident non-linear ultrasound wave at the droplet location should be computed. Next, for each harmonic, the diffraction problem should be solved in terms of spherical harmonics. Adding the diffracted waves inside the droplet with the proper amplitude and phase will then yield the total pressure in the droplet. Figure 1 illustrates that

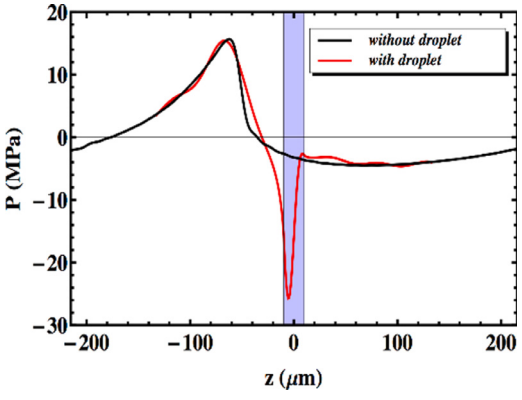

Fig. 1. Combined effect of non-linear propagation and focusing of the harmonics in a perfluoropentane micrometer-sized droplet. The emitted ultrasound wave has a frequency of 3.5 MHz and a focus at 3.81 cm, and the radius of the droplet is 10 μm for ease of observation. The pressures are given on the axis of the droplet along the propagating direction of the

the combined effects of non-linear propagation and diffraction can cause a dramatic amplification of the peak negative pressure in the micrometer-sized droplet, sufficient for triggering droplet vaporization (Shpak et al. 2014). Moreover, the location of the negative pressure peak also agrees with the observed nucleation spot.

After vaporization has started, the growth of the emerging bubble is limited by inertia and heat transfer. In the absence of the heat transfer limitation, the inertia of the fluid that surrounds the bubble limits the rate of bubble growth, which is linearly proportional to time and inversely proportional to the square root of the density of the surrounding fluid. When inertia is neglected, thermal diffusion is the limiting factor in the transport of heat to drive the endothermic vaporization process of perfluorocarbon, causing the radius of the bubble to increase with the square root of time. In reality, both processes occur simultaneously, where the inertia effect is dominant at the early stage and the diffusion effect is dominant at the later stage of bubble growth. The final size that is reached by a bubble depends on the time that a bubble can expand, that is, on the duration of the negative cycle of the insonifying pressure wave. It is therefore expected that lower insonification frequencies give rise to larger maximum bubble size. Thus, irrespective of their influence on triggering ADV, lower frequencies would lead to more violent inertial cavitation effects and cause more biological damage, as experimentally observed for droplets with a radius in the order of 100 nm (Burgess and Porter 2019).

Biological mechanisms and bio-effects of ultrasound-activated cavitation nuclei

The biological phenomena of sonoporation (*i.e.,* membrane pore formation), stimulated endocytosis and opening of cell−cell contacts and the bio-effects of intracellular calcium transients, ROS generation, cell membrane potential change and cytoskeleton changes have been observed for several years (Sutton et al. 2013; Kooiman et al. 2014; Lentacker et al. 2014; Qin et al. 2018b). However, other bio-effects induced by ultrasound-activated cavitation nuclei have recently been discovered. These include membrane blebbing as a recovery mechanism for reversible sonoporation (both for ultrasound-activated microbubbles [Leow et al. 2015] and upon ADV [Qin et al. 2018a]), extracellular vesicle formation (Yuana et al. 2017), suppression of efflux transporter P-glycoprotein (Cho et al. 2016; Aryal et al. 2017) and BBB (blood−brain barrier) transporter genes (McMahon et al. 2018). At the same time, more insight has been gained into the origin of the bio-effects, largely through the use of live cell microscopy. For sonoporation, real-time membrane pore opening and closure dynamics were revealed with pores $<30\ \mu m^2$ closing within 1 min, while pores $>100\ \mu m^2$ did not reseal (Hu et al. 2013) as well as immediate rupture of filamentary actin at the pore location (Chen et al. 2014) and correlation of intracellular ROS levels with the degree of sonoporation (Jia et al. 2018). Real-time sonoporation and opening of cell−cell contacts in the same endothelial cells have been reported as well for a single example (Helfield et al. 2016). The applied acoustic pressure was found to determine uptake of model drugs *via* sonoporation or endocytosis in another study (De Cock et al. 2015). Electron microscopy revealed formation of transient membrane disruptions and permanent membrane structures, that is, caveolar endocytic vesicles, upon ultrasound and microbubble treatment (Zeghimi et al. 2015). A study by Fekri et al. (2016) revealed that enhanced clathrin-mediated endocytosis and fluid-phase endocytosis occur through distinct signaling mechanisms upon ultrasound and microbubble treatment. The majority of these bio-effects have been observed in *in vitro* models using largely non-endothelial cells and may therefore not be directly relevant to *in vivo* tissue, where intravascular micron-sized cavitation nuclei will only have contact with endothelial cells and circulating blood cells. On the other hand, the mechanistic studies by Belcik et al. (2015, 2017) and Yu et al. (2017) do reveal translation from *in vitro* to *in vivo*. In these studies, ultrasound-activated microbubbles were found to induce a shear-dependent increase in intravascular adenosine triphosphate (ATP) from both endothelial cells and erythrocytes, an increase in intramuscular nitric oxide and downstream signaling through both nitric oxide and prostaglandins, which resulted in augmentation of muscle blood flow. Ultrasound settings were similar, namely, 1.3 MHz, mechanical index (MI) 1.3 for Belcik et al. (2015, 2017) and 1 MHz, MI 1.5 for Yu et al. (2017), with MI defined as $MI = P\_/\sqrt{f}$, where $P\_$ is the derated peak negative pressure of the ultrasound wave (in MPa) and f the center frequency of the ultrasound wave (in MHz).

Whether or not there is a direct relationship between the type of microbubble oscillation and specific bio-effects remains to be elucidated, although more insight has been gained through ultrahigh-speed imaging of the microbubble behavior in conjunction with live cell microscopy. For example, there seems to be a microbubble excursion threshold above which sonoporation occurs (Helfield et al. 2016). Van Rooij et al. (2016) further found that displacement of targeted microbubbles enhanced reversible sonoporation and preserved cell viability, whilst microbubbles that did not displace were identified as the main contributors to cell death.

All of the aforementioned biological observations, mechanisms and effects relate to eukaryotic cells. Study of the biological effects of cavitation on, for example,

bacteria is in its infancy, but studies suggest that sonoporation can be achieved in Gram-negative bacteria, with dextran uptake and gene transfection being reported in *Fusobacterium nucleatum* (Han et al. 2007). More recent studies have investigated the effect of microbubbles and ultrasound on gene expression (Li et al. 2015; Dong et al. 2017; Zhou et al. 2018). The findings are conflicting because although they all reveal a reduction in expression of genes involved in biofilm formation and resistance to antibiotics, an increase in expression of genes involved with dispersion and detachment of biofilms was also found (Dong et al. 2017). This cavitation-mediated bio-effect needs further investigation.

Modelling microbubble−cell−drug interaction

Whilst there have been significant efforts to model the dynamics of ultrasound-driven microbubbles (Faez et al. 2013; Dollet et al. 2019), less attention has been paid to the interactions between microbubbles and cells or their impact upon drug transport. Currently there are no models that describe the interactions between microbubbles, cells and drug molecules. Several models have been proposed for the microbubble−cell interaction in sonoporation focusing on different aspects: cell expansion and microbubble jet velocity (Guo et al. 2017b), the shear stress exerted on the cell membrane (Wu 2002; Doinikov and Bouakaz 2010; Forbes and O'Brien 2012; Yu and Chen 2014; Cowley and McGinty 2019), microstreaming (Yu and Chen 2014), the shear stress exerted on the cell membrane in combination with microstreaming (Li et al. 2014) or other flow phenomena (Yu et al. 2015; Rowlatt and Lind 2017) generated by an oscillating microbubble. In contrast to the other models, Man et al. (2019) propose that the microbubble-generated shear stress does not induce pore formation, but is instead due to microbubble fusion with the membrane and subsequent "pull out" of cell membrane lipid molecules by the oscillating microbubble. Models for pore formation (*e.g.,* Koshiyama and Wada 2011) and resealing (Zhang et al. 2019) in cell membranes have also been developed, but these models neglect the mechanism by which the pore is created. There is just one sonoporation dynamics model, developed by Fan et al. (2012), that relates the uptake of the model drug propidium iodide (PI) to the size of the created membrane pore and the pore resealing time for a single cell in an *in vitro* setting. The model describes the intracellular fluorescence intensity of PI as a function of time, *F(t)*, by

$$F(t) = \alpha \cdot \pi D C_0 \cdot r_o \cdot \frac{1}{\beta}\left(1 - e^{-\beta t}\right) \quad (3)$$

where α is the coefficient that relates the amount of PI molecules to the fluorescence intensity of PI-DNA and PI-RNA, D is the diffusion coefficient of PI, C_0 is the extracellular PI concentration, r_0 is the initial radius of the pore, β is the pore re-sealing coefficient and t is time. The coefficient α is determined by the sensitivity of the fluorescence imaging system, and if unknown, the equation can still be used because it is the pore size coefficient, $\alpha \cdot \pi D C_0 \cdot r_0$, that determines the initial slope of the PI uptake pattern and is the scaling factor for the exponential increase. A cell with a large pore will have a steep initial slope of PI uptake, and the maximum PI intensity quickly reaches the plateau value. A limitation of this model is that eqn (3) is based on 2-D free diffusion models, which holds for PI-RNA but not for PI-DNA because the latter is confined to the nucleus. The model is independent of cell type, as Fan et al. have reported agreement with experimental results in both kidney (Fan et al. 2012) and endothelial cells (Fan et al. 2013). Other researchers have also used this model for endothelial cell studies and also classified the distribution of both the pore size and pore resealing coefficients using principal component analysis (PCA) to determine whether cells were reversibly or irreversibly sonoporated. In the context of BBB opening, Hosseinkhah et al. (2015) have modeled the microbubble-generated shear and circumferential wall stress for 5-μm microvessels upon microbubble oscillation at a fixed MI of 0.134 for a range of frequencies (0.5, 1 and 1.5 MHz). The wall stresses were dependent upon microbubble size (range investigated: 2−18 μm in diameter) and ultrasound frequency. Wiedemair et al. (2017) have also modelled the wall shear stress generated by microbubble (2 μm in diameter) destruction at 3 MHz for larger microvessels (200 μm in diameter). The presence of red blood cells was included in the model and was found to cause confinement of pressure and shear gradients to the vicinity of the microbubble. Advances in methods for imaging microbubble−cell interactions will facilitate the development of more sophisticated mechanistic models.

TREATMENT OF TUMORS (NON-BRAIN)

The structure of tumor tissue varies significantly from that of healthy tissue which has important implications for its treatment. To support the continuous expansion of neoplastic cells, the formation of new vessels (*i.e.,* angiogenesis) is needed (Junttila and de Sauvage 2013). As such, a rapidly developed, poorly organized vasculature with enlarged vascular openings arises. Between these vessels, large avascular regions exist, which are characterized by a dense extracellular matrix, high interstitial pressure, low pH and hypoxia. Moreover, a local immunosuppressive environment is formed, preventing possible anti-tumor activity by the immune system.

Notwithstanding the growing knowledge of the pathophysiology of tumors, treatment remains challenging. Chemotherapeutic drugs are typically administered to abolish the rapidly dividing cancer cells. Yet, their cytotoxic effects are not limited to cancer cells, causing dose-limiting off-target effects. To overcome this hurdle, chemotherapeutics are often encapsulated in nano-sized carriers, that is, nanoparticles, that are designed to specifically diffuse through the large openings of tumor vasculature, while being excluded from healthy tissue by normal blood vessels (Lammers et al. 2012; Maeda 2012). Despite being highly promising in pre-clinical studies, drug-containing nanoparticles have exhibited limited clinical success because of the vast heterogeneity in tumor vasculature (Barenholz 2012; Lammers et al. 2012; Wang et al. 2015d). In addition, drug penetration into the deeper layers of the tumor can be constrained by high interstitial pressure and a dense extracellular matrix in the tumor. Furthermore, acidic and hypoxic regions limit the efficacy of radiation- and chemotherapy-based treatments because of biochemical effects (Mehta et al. 2012; McEwan et al. 2015; Fix et al. 2018). Ultrasound-triggered microbubbles are able to alter the tumor environment locally, thereby improving drug delivery to tumors. These alterations are schematically represented in Figure 2 and include improving vascular permeability, modifying the tumor perfusion, reducing local hypoxia and overcoming the high interstitial pressure.

Several studies have found that ultrasound-driven microbubbles improved delivery of chemotherapeutic agents in tumors, which resulted in increased anti-tumor effects (Wang et al. 2015d; Snipstad et al. 2017; Zhang et al. 2018). Moreover, several gene products could be effectively delivered to tumor cells *via* ultrasound-driven microbubbles, resulting in a downregulation of tumor-specific pathways and an inhibition in tumor growth (Kopechek et al. 2015; Zhou et al. 2015). Theek et al. (2016) furthermore confirmed that nanoparticle accumulation can be achieved in tumors with low EPR effect. Drug transport and distribution through the dense tumor matrix and into regions with elevated interstitial pressure are often the limiting factors in peripheral tumors. As a result, several reports have indicated that drug penetration into the tumor remained limited after sonoporation, which may impede the eradication of the entire tumor tissue (Eggen et al. 2014; Wang et al. 2015d; Wei et al. 2019). Alternatively, microbubble cavitation can affect

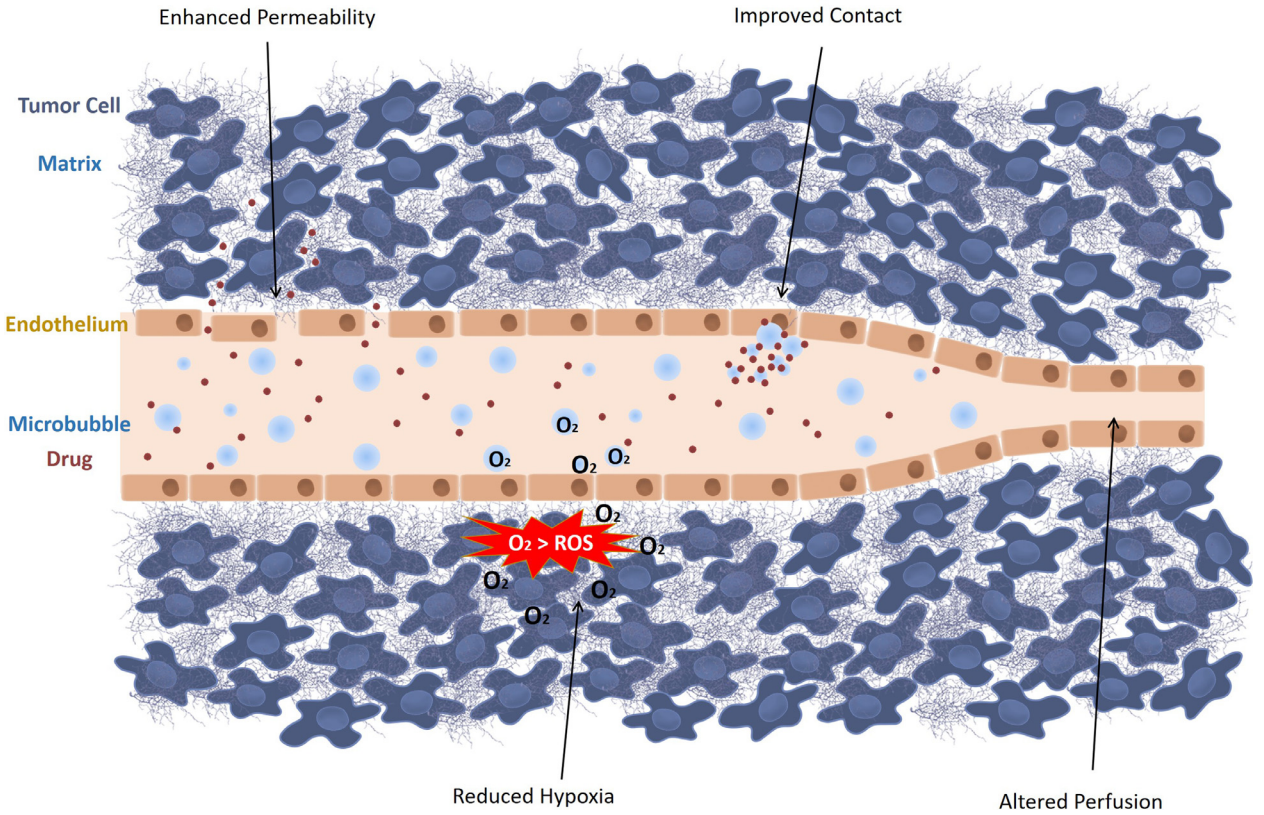

Fig. 2. Ultrasound-activated microbubbles can locally alter the tumor microenvironment through four mechanisms: enhanced permeability, improved contact, reduced hypoxia and altered perfusion. ROS = reactive oxygen species.

tumor perfusion, as vasoconstriction and even temporary vascular shutdown have been reported *ex vivo* (Keravnou et al. 2016) and *in vivo* (Hu et al. 2012; Goertz 2015; Yemane et al. 2018). These effects were seen at higher ultrasound intensities (>1.5 MPa) and are believed to result from inertial cavitation leading to violent microbubble collapses. As blood supply is needed to maintain tumor growth, vascular disruption might form a different approach to cease tumor development. Microbubble-induced microvascular damage was able to complement the direct effects of chemotherapeutics and antivascular drugs by secondary ischemia-mediated cytotoxicity, which led to tumor growth inhibition (Wang et al. 2015a; Ho et al. 2018; Yang et al. 2019b). In addition, a synergistic effect between radiation therapy and ultrasound-stimulated microbubble treatment was observed, as radiation therapy also induces secondary cell death by endothelial apoptosis and vascular damage (Lai et al. 2016; Daecher et al. 2017). Nevertheless, several adverse effects have been reported because of excessive vascular disruption, including hemorrhage, tissue necrosis and the formation of thrombi (Goertz 2015; Wang et al. 2015d; Snipstad et al. 2017).

Furthermore, oxygen-containing microbubbles can provide a local oxygen supply to hypoxic areas, rendering oxygen-dependent treatments more effective. This is of interest for sonodynamic therapy, which is based on the production of cytotoxic ROS by a sonosensitizing agent upon activation by ultrasound in the presence of oxygen (McEwan et al. 2015, 2016; Nesbitt et al. 2018). As ultrasound can be used to stimulate the release of oxygen from oxygen-carrying microbubbles while simultaneously activating a sonosensitizer, this approach has been reported to be particularly useful for the treatment of hypoxic tumor types (McEwan et al. 2015; Nesbitt et al. 2018). Additionally, low oxygenation promotes resistance to radiotherapy, which can be circumvented by a momentary supply of oxygen. Based on this notion, oxygen-carrying microbubbles were used to improve the outcome of radiotherapy in a rat fibrosarcoma model (Fix et al. 2018).

Finally, ultrasound-activated microbubbles promote convection and induce acoustic radiation forces. As such, closer contact with the tumor endothelium and an extended contact time can be obtained (Kilroy et al. 2014). Furthermore, these forces may counteract the elevated interstitial pressure present in tumors (Eggen et al. 2014; Lea-Banks et al. 2016; Xiao et al. 2019).

Apart from their ability to improve tumor uptake, microbubbles can be used as ultrasound-responsive drug carriers to reduce the off-target effects of chemotherapeutics. By loading the drugs or drug-containing nanoparticles directly into or onto the microbubbles, a spatial and temporal control of drug release can be obtained, thereby reducing exposure to other parts of the body (Yan et al. 2013; Snipstad et al. 2017). Moreover, several studies have reported improved anti-cancer effects from treatment with drug-coupled microbubbles, compared with a co-administration approach (Burke et al. 2014; Snipstad et al. 2017). Additionally, tumor neovasculature expresses specific surface receptors that can be targeted by specific ligands. Adding such targeting moieties to the surface of (drug-loaded) microbubbles improves site-targeted delivery and has been found to potentiate this effect further (Bae et al. 2016; Xing et al. 2016; Luo et al. 2017).

Phase-shifting droplets and gas-stabilizing solid agents (*e.g.,* nanocups) have the unique ability to benefit from both EPR-mediated accumulation in the "leaky" parts of the tumor vasculature because of their small sizes, as well as from ultrasound-induced permeabilization of the tissue structure (Zhou 2015; Myers et al. 2016; Liu et al. 2018b; Zhang et al. 2018). Several research groups have reported tumor regression after treatment with acoustically active droplets (Gupta et al. 2015; van Wamel et al. 2016; Cao et al. 2018; Liu et al. 2018b) or gas-stabilizing solid particles (Min et al. 2016; Myers et al. 2016). A different approach to the use of droplets for tumor treatment is ACT, which is based on microbubble-droplet clusters that upon ultrasound exposure, undergo a phase shift to create large bubbles that can transiently block capillaries (Sontum et al. 2015). Although the mechanism behind the technique is not yet fully understood, studies have reported improved delivery and efficacy of paclitaxel and Abraxane in xenograft prostate tumor models (van Wamel et al. 2016; Kotopoulis et al. 2017). Another use of droplets for tumor treatment is enhanced high-intensity focused ultrasound (HIFU)-mediated heating of tumors (Kopechek et al. 2014).

Although microbubble-based drug delivery to solid tumors shows great promise, it also faces important challenges. The ultrasound parameters used in *in vivo* studies highly vary between research groups, and no consensus was found on the oscillation regime that is believed to be responsible for the observed effects (Wang et al. 2015d; Snipstad et al. 2017). Moreover, longer ultrasound pulses and increased exposure times are usually applied in comparison to *in vitro* reports (Roovers et al. 2019c). This could promote additional effects such as microbubble clustering and microbubble translation, which could cause local damage to the surrounding tissue as well (Roovers et al. 2019a). To elucidate these effects further, fundamental *in vitro* research remains important. Therefore, novel *in vitro* models that more accurately mimic the complexity of the *in vivo* tumor environment are currently being explored. Park et al. (2016) engineered a perfusable vessel-on-a-chip system and reported

successful doxorubicin delivery to the endothelial cells lining this microvascular network. While such microfluidic chips could be extremely useful to study the interactions of microbubbles with the endothelial cell barrier, special care of the material of the chambers should be taken to avoid ultrasound reflections and standing waves (Beekers et al. 2018). Alternatively, 3-D tumor spheroids have been used to study the effects of ultrasound and microbubble-assisted drug delivery on penetration and therapeutic effect in a multicellular tumor model (Roovers et al. 2019b). Apart from expanding the knowledge on microbubble−tissue interactions in detailed parametric studies *in vitro*, it will be crucial to obtain improved control over the microbubble behavior *in vivo*, and link this to the therapeutic effects. To this end, passive cavitation detection to monitor microbubble cavitation behavior in real time is currently under development, and could provide better insights in the future (Choi et al. 2014; Graham et al. 2014; Haworth et al. 2017). Efforts are being committed to construction of custom-built delivery systems, which can be equipped with multiple transducers allowing drug delivery guided by ultrasound imaging and/or passive cavitation detection (Escoffre et al. 2013; Choi et al. 2014; Wang et al. 2015c; Paris et al. 2018).

Clinical studies

Pancreatic cancer. The tolerability and therapeutic potential of improved chemotherapeutic drug delivery using microbubbles and ultrasound were first investigated for the treatment of inoperable pancreatic ductal adenocarcinoma at Haukeland University Hospital, Norway (Kotopoulis et al. 2013; Dimcevski et al. 2016). In this clinical trial, gemcitabine was administered by intravenous injection over 30 min. During the last 10 min of chemotherapy, an abdominal echography was performed to locate the position of pancreatic tumor. At the end of chemotherapy, 0.5 mL of SonoVue microbubbles followed by 5 mL saline was intravenously injected every 3.5 min to ensure their presence throughout the whole sonoporation treatment. Pancreatic tumors were exposed to ultrasound (1.9 MHz, MI 0.2, 1% DC) using a 4C curvilinear probe (GE Healthcare) connected to an LOGIQ 9 clinical ultrasound scanner. The cumulative ultrasound exposure was only 18.9 s. All clinical data indicated that microbubble-mediated gemcitabine delivery did not induce any serious adverse events in comparison to chemotherapy alone. At the same time, tumor size and development were characterized according to the Response Evaluation Criteria in Solid Tumors (RECIST) criteria. In addition, Eastern Cooperative Oncology Group performance status was used to monitor the therapeutic efficacy of microbubble-mediated gemcitabine delivery. All 10 patients tolerated an increased number of gemcitabine cycles compared with treatment with chemotherapy alone from historical controls (8.3 ± 6 vs. 13.8 ± 5.6 cycles, $p < 0.008$), thus reflecting an improved physical state. After 12 treatment cycles, one patient's tumor exhibited a twofold decrease in tumor size. This patient was excluded from this clinical trial to be treated with radiotherapy and then with pancreatectomy. In 5 of the 10 patients, the maximum tumor diameter was partially decreased from the first to last therapeutic treatment. Subsequently, a consolidative radiotherapy or a FOLFIRINOX treatment, a bolus and infusion of 5-fluorouracil, leucovorin, irinotecan and oxaliplatin, was offered to them. The median survival was significantly increased from 8.9 to 17.6 mo ($p = 0.0001$). Together, these results indicate that drug delivery using clinically approved microbubbles, chemotherapeutics and ultrasound is feasible and compatible with respect to clinical procedures. Nevertheless, the authors did not provide any evidence that the improved therapeutic efficacy of gemcitabine was related to an increase in intra-tumoral bioavailability of the drug. In addition, the effects of microbubble-assisted ultrasound treatment alone on tumor growth were not investigated, while recent publications describe that according to the ultrasound parameters, such treatment could induce a significant decrease in tumor volume through a reduction in tumor perfusion as described above.

Hepatic metastases from the digestive system. A tolerability study of chemotherapeutic delivery using microbubble-assisted ultrasound for the treatment of liver metastases from gastrointestinal tumors and pancreatic carcinoma was conducted at Beijing Cancer Hospital, China (Wang et al. 2018). Thirty minutes after intravenous infusion of chemotherapy (for both monotherapy and combination therapy), 1 mL of SonoVue microbubbles was intravenously administered and was repeated another five times in 20 min. An ultrasound probe (C1-5 abdominal convex probe; GE Healthcare, USA) was positioned on the tumor lesion, which was exposed to ultrasound at different MIs (0.4−1) in contrast mode using a LogiQ E9 scanner (GE Healthcare, USA). The primary aims of this clinical trial were to evaluate the tolerability of this therapeutic procedure and to explore the largest MI and ultrasound treatment time that cancer patients can tolerate. According to the clinical tolerability evaluation, all 12 patients exhibited no serious adverse events. The authors reported that the microbubble-mediated chemotherapy led to fever in 2 patients. However, there is no clear evidence this is related to the microbubble and ultrasound treatment. Indeed, in the absence of direct comparison of these results with a historical group of patients receiving the

chemotherapy on its own, one cannot rule out a direct link between the fever and the chemotherapy alone. All adverse side effects were resolved with symptomatic medication. In addition, the severity of side effects did not worsen with increases in MI, suggesting that microbubble-mediated chemotherapy is a tolerable procedure. The secondary aims were to assess the efficacy of this therapeutic protocol using contrast-enhanced computed tomography (CT) and magnetic resonance imaging (MRI). Thus, tumor size and development were characterized according to the RECIST criteria. Half of the patients had stable disease, and one patient obtained a partial response after the first treatment cycle. The median progression-free survival was 91 d. However, comparison and interpretation of results are very difficult because none of the patients were treated with the same chemotherapeutics, MI and/or number of treatment cycles. The results of tolerability and efficacy evaluations should be compared with those for patients receiving the chemotherapy on its own to clearly identify the therapeutic benefit of combining therapy with ultrasound-driven microbubbles. Similar to the pancreatic clinical study, no direct evidence of enhanced therapeutic bioavailability of the chemotherapeutic drug after the treatment was provided. This investigation is all the more important as the ultrasound and microbubble treatment was applied 30 min after intravenous chemotherapy (for both monotherapy and combination therapy) independently of drug pharmacokinetics and metabolism.

Ongoing and upcoming clinical trials. Currently, two clinical trials are ongoing: (i) Professor F. Kiessling (RWTH Aachen University, Germany) proposes examining whether the exposure of early primary breast cancer to microbubble-assisted ultrasound during neoadjuvant chemotherapy results in increased tumor regression in comparison to that after ultrasound treatment alone (NCT03385200). (ii) Dr. J. Eisenbrey (Sidney Kimmel Cancer Center, Thomas Jefferson University, USA) is investigating the therapeutic potential of perflutren protein type A microspheres in combination with microbubble-assisted ultrasound in radioembolization therapy of liver cancer (NCT03199274).

A proof of concept study (NCT03458975) has been set in Tours Hospital, France, for treating non-resectable liver metastases. The aim of this trial is to perform a feasibility study with the development of a dedicated ultrasound imaging and delivery probe with a therapy protocol optimized for patients with hepatic metastases of colorectal cancer and who are eligible for monoclonal antibodies in combination with chemotherapy. A dedicated 1.5-D ultrasound probe has been developed and interconnected to a modified Aixplorer imaging platform (Supersonic Imagine, Aix-en-Provence, France). The primary objective of the study is to determine the rate of objective response at 2 mo for lesions receiving optimized and targeted delivery of systemic chemotherapy combining bevacizumab and FOLFIRI compared with those treated with only the systemic chemotherapy regimen. The secondary objective is to determine the tolerability of this local approach of optimized intra-tumoral drug delivery during the 3 mo of follow-up, by assessing tumor necrosis, tumor vascularity and pharmacokinetics of bevacizumab and by profiling cytokine expression spatially.

IMMUNOTHERAPY

Cancer immunotherapy is considered to be one of the most promising strategies to eradicate cancer as it makes use of the patient's own immune system to selectively attack and destroy tumor cells. It is a common name that refers to a variety of strategies that aim to unleash the power of the immune system by either boosting antitumoral immune responses or flagging tumor cells to make them more visible to the immune system. The principle is that tumors express specific tumor antigens which are not expressed or expressed to a much lesser extent by normal somatic cells and hence can be used to initiate a cancer-specific immune response. In this section we aim to give insight into how microbubbles and ultrasound have been applied as useful tools to initiate or sustain different types of cancer immunotherapy, as illustrated in Figure 3.

When Ralph Steinman (Steinman et al. 1979) discovered the dendritic cell (DC) in 1973, its central role in the initiation of immunity made it an attractive target to evoke specific antitumoral immune responses. Indeed, these cells very efficiently capture antigens and present them to T lymphocytes in major histocompatibility complexes (MHCs), thereby bridging the innate and adaptive immune systems. More specifically, exogenous antigens engulfed *via* the endolysosomal pathway are largely presented to $CD4^+$ T cells *via* MHC-II, whereas endogenous, cytoplasmic proteins are shuttled to MHC-I molecules for presentation to $CD8^+$ cells. As such, either $CD4^+$ helper T cells or $CD8^+$ cytotoxic T-cell responses are induced. The understanding of this pivotal role played by DCs formed the basis for DC-based vaccination, where a patient's DCs are isolated, modified *ex vivo* to present tumor antigens and re-administered as a cellular vaccine. DC-based therapeutics, however, suffer from a number of challenges, of which the expensive and lengthy *ex vivo* procedure for antigen loading and activation of DCs is the most prominent (Santos and Butterfield 2018). In this regard, microbubbles have been investigated for direct delivery of tumor antigens to

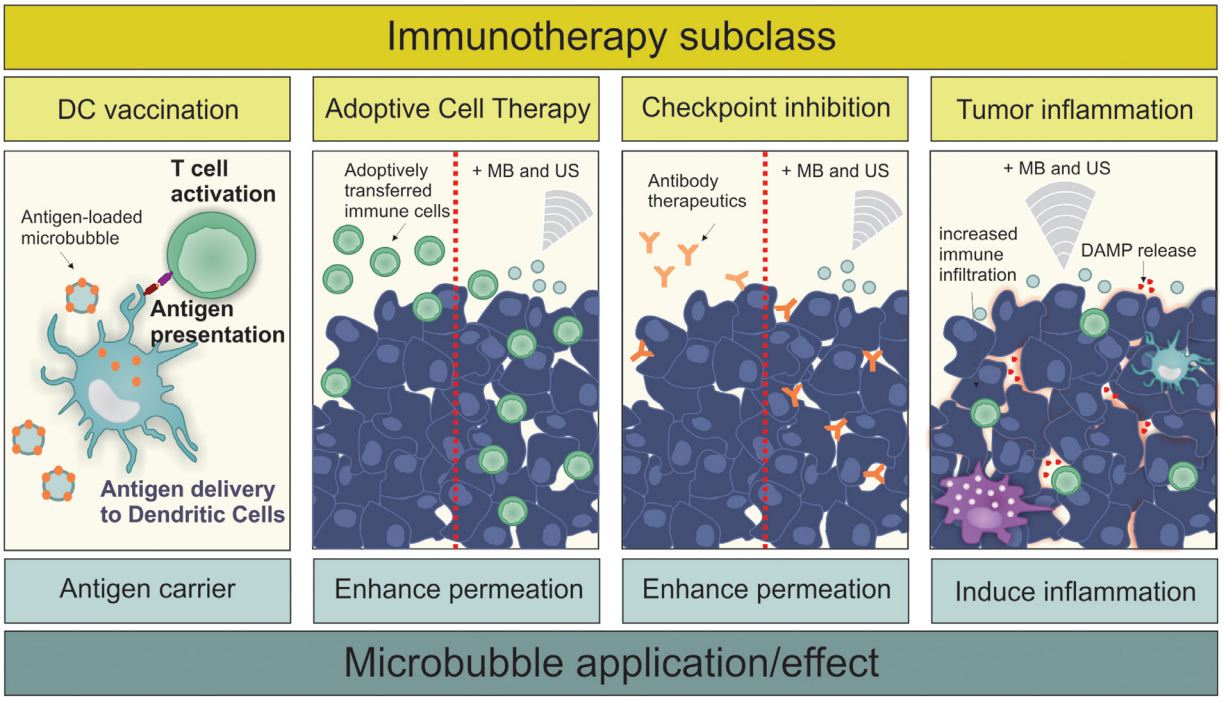

Fig. 3. Schematic overview of how microbubbles (MB) and ultrasound (US) have been found to contribute to cancer immunotherapy. From left to right: Microbubbles can be used as antigen carriers to stimulate antigen uptake by dendritic cells. Microbubbles and ultrasound can alter the permeability of tumors, thereby increasing the intra-tumoral penetration of adoptively transferred immune cells or checkpoint inhibitors. Finally, exposing tissues to cavitating microbubbles can induce sterile inflammation by the local release of damage-associated molecular patterns (DAMPS).

immune cells *in vivo*. Bioley et al. (2015) reported that intact microbubbles are rapidly phagocytosed by both murine and human DCs, resulting in rapid and efficient uptake of surface-coupled antigens without the use of ultrasound. Subcutaneous injection of microbubbles loaded with the model antigen ovalbumin (OVA) resulted in the activation of both $CD8^+$ and $CD4^+$ T cells. Effectively, these T-cell responses could partially protect vaccinated mice against an OVA-expressing *Listeria* infection. Dewitte et al. (2014) investigated a different approach, making use of messenger RNA (mRNA)-loaded microbubbles combined with ultrasound to transfect DCs. As such, they were able to deliver mRNA encoding both tumor antigens and immunomodulating molecules directly to the cytoplasm of the DCs. As a result, preferential presentation of antigen fragments in MHC-I complexes was ensured, favoring the induction of $CD8^+$ cytotoxic T cells. In a therapeutic vaccination study in mice bearing OVA-expressing tumors, injection of mRNA-sonoporated DCs caused a pronounced slowdown of tumor growth and induced complete tumor regression in 30% of the vaccinated animals. Interestingly, in humans, intradermally injected microbubbles have been used as sentinel lymph node detectors as they can easily drain from peripheral sites to the afferent lymph nodes (Sever et al. 2012a, 2012b). As lymph nodes are the primary sites of immune induction, the interaction of microbubbles with intranodal DCs, could be of high value. To this end, Dewitte et al. (2015) found that mRNA-loaded microbubbles were able to rapidly and efficiently migrate to the afferent lymph nodes after intradermal injection in healthy dogs. Unfortunately, further translation of this concept to an *in vivo* setting is not straightforward, as it prompts the use of less accessible large animal models (*e.g.,* pigs, dogs). Indeed, conversely to what has been reported in humans, lymphatic drainage of subcutaneously injected microbubbles is very limited in the small animal models typically used in pre-clinical research (mice and rats), which is the result of substantial differences in lymphatic physiology.

Another strategy in cancer immunotherapy is adoptive cell therapy, in which *ex vivo* manipulated immune effector cells, mainly T cells and natural killer (NK) cells, are employed to generate a robust and selective anticancer immune response (Yee 2018; Hu et al. 2019). These strategies have mainly led to successes in hematological malignancies, not only because of the availability of selective target antigens, but also because of the accessibility of the malignant cells (Khalil et al. 2016; Yee 2018). By contrast, in solid tumors, and especially

in brain cancers, inadequate homing of cytotoxic T cells or NK cells to the tumor proved to be one of the main reasons for the low success rates, making the degree of tumor infiltration an important factor in disease prognosis (Childs and Carlsten 2015; Gras Navarro et al. 2015; Yee 2018). To address this, focused ultrasound and microbubbles have been used to make tumors more accessible to cellular therapies. The first demonstration of this concept was provided by Alkins et al. (2013), who used a xenograft HER-2-expressing breast cancer brain metastasis model to determine whether ultrasound and microbubbles could allow intravenously infused NK cells to cross the BBB. By loading the NK cells with superparamagnetic iron oxide nanoparticles, the accumulation of NK cells in the brain could be tracked and quantified *via* MRI. An enhanced accumulation of NK cells was found when the cells were injected immediately before BBB disruption. Importantly NK cells retained their activity and ultrasound treatment resulted in a sufficient NK-to-tumor cell ratio to allow effective tumor cell killing (Alkins et al. 2016). In contrast, very few NK cells reached the tumor site when BBB disruption was absent or performed before NK cell infusion. Although it is not known for certain why timing had such a significant impact on NK extravasation, it is likely that the most effective transfer to the tissue occurs at the time of insonification, and that the barrier is most open during this time (Marty et al. 2012). Possible other explanations include the difference in size of the temporal BBB openings or a possible alternation in the expression of specific leukocyte adhesion molecules by the BBB disruption, thus facilitating the translocation of NK cells. Also, for tumors where BBB crossing is not an issue, ultrasound has been used to improve delivery of cellular therapeutics. Sta Maria et al. (2015) reported enhanced tumor infiltration of adoptively transferred NK cells after treatment with microbubbles and low-dose focused ultrasound. This result was confirmed by Yang et al. (2019a) in a more recent publication where the homing of NK cells more than doubled after microbubble injection and ultrasound treatment of an ovarian tumor. Despite the enhanced accumulation, however, the authors did not observe an improved therapeutic effect, which might be owing to the limited number of treatments that were applied or the immunosuppressive tumor microenvironment that counteracts the cytotoxic action of the NK cells.

There is growing interest in exploring the effect of microbubbles and ultrasound on the tumor microenvironment, as recent work has indicated that BBB disruption with microbubbles and ultrasound may induce sterile inflammation. Although a strong inflammatory response may be detrimental in the case of drug delivery across the BBB, it might be interesting to further study this inflammatory response in solid tumors as it might induce the release of damage-associated molecular patterns (DAMPS) such as heat-shock proteins and inflammatory cytokines. This could shift the balance toward a more inflammatory microenvironment that could promote immunotherapeutic approaches. As reported by Liu et al. (2012) exposure of a CT26 colon carcinoma xenograft to microbubbles and low-pressure pulsed ultrasound increased cytokine release and triggered lymphocyte infiltration. Similar data have been reported by Hunt et al. (2015). In their study, ultrasound treatment caused a complete shutdown of tumor vasculature followed by the expression of hypoxia-inducible factor 1α (HIF-1α), a marker of tumor ischemia and tumor necrosis, as well as increased infiltration of T cells. Similar responses have been reported after thermal and mechanical HIFU treatments of solid tumors (Unga and Hashida 2014; Silvestrini et al. 2017). A detailed review of ablative ultrasound therapies is, however, out of the scope of this review.

At present, the most successful form of immunotherapy is the administration of monoclonal antibodies to inhibit regulatory immune checkpoints that block T-cell action. Examples are cytotoxic T lymphocyte-associated protein 4 (CTLA-4) and programmed cell death 1 (PD-1), which act as brakes on the immune system. Blocking the effect of these brakes can revive and support the function of immune effector cells. Despite the numerous successes achieved with checkpoint inhibitors, responses have been quite heterogeneous as the success of checkpoint inhibition therapy depends largely on the presence of intra-tumoral effector T cells (Weber 2017). This motivated Bulner et al. (2019) to explore the synergy of microbubble and ultrasound treatment with PD-L1 checkpoint inhibition therapy in mice. Tumors in the treatment group that received the combination of microbubble and ultrasound treatment with checkpoint inhibition were significantly smaller than tumors in the monotherapy groups. One mouse exhibited complete tumor regression and remained tumor free upon rechallenge, indicative of an adaptive immune response.

Overall, the number of studies that have investigated the impact of microbubble and ultrasound treatment on immunotherapy is limited, making this a rather unexplored research area. It is obvious that more in-depth research is warranted to improve our understanding on how (various types of) immunotherapy might benefit from (various types of) ultrasound treatment.

BBB AND BLOOD–SPINAL CORD BARRIER OPENING

The barriers of the central nervous system (CNS), the BBB and blood–spinal cord barrier (BSCB), greatly

limit drug-based treatment of CNS disorders. These barriers help to regulate the specialized CNS environment by limiting the passage of most therapeutically relevant molecules (Pardridge 2005). Although several methods have been proposed to circumvent the BBB and BSCB, including chemical disruption and the development of molecules engineered to capitalize on receptor-mediated transport (so-called Trojan horse molecules), the use of ultrasound in combination with microbubbles (Hynynen et al. 2001) or droplets (Wu et al. 2018) to transiently modulate these barriers has come to the forefront in recent years because of the targeted nature of this approach and its ability to facilitate delivery of a wide range of currently available therapeutics. First demonstrated in 2001 (Hynynen et al. 2001), ultrasound-mediated BBB opening has been the topic of several hundred original research articles in the last two decades and, in recent years, has made headlines for groundbreaking clinical trials targeting brain tumors and Alzheimer's disease as described later under Clinical Studies.

Mechanisms, bio-effects and tolerability

Ultrasound in combination with microbubbles can produce permeability changes in the BBB *via* both enhanced paracellular and transcellular transport (Sheikov et al. 2004, 2006). Reduction and reorganization of tight junction proteins (Sheikov et al. 2008) and upregulation of active transport protein caveolin-1 (Deng et al. 2012) have been reported. Although the exact physical mechanisms driving these changes are not known, there are several factors that are hypothesized to contribute to these effects, including direct tensile stresses caused by the expansion and contraction of the bubbles in the lumen, as well as shear stresses at the vessel wall arising from acoustic microstreaming. Recent studies have also investigated the suppression of efflux transporters after ultrasound exposure with microbubbles. A reduction in P-glycoprotein expression (Cho et al. 2016; Aryal et al. 2017) and BBB transporter gene expression (McMahon et al. 2018) has been observed by multiple groups. One study found that P-glycoprotein expression was suppressed for more than 48 h after treatment with ultrasound and microbubbles (Aryal et al. 2017). However, the degree of inhibition of efflux transporters as a result of ultrasound with microbubbles may be insufficient to prevent efflux of some therapeutics (Goutal et al. 2018), and thus this mechanism requires further study.

Many studies have documented enhanced CNS tumor response after ultrasound and microbubble-mediated delivery of drugs across the blood−tumor barrier in rodent models. Improved survival has been observed in both primary (Chen et al. 2010; Aryal et al. 2013) and metastatic (Park et al. 2012; Alkins et al. 2016) tumor models.

Beyond simply enhancing drug accumulation in the CNS, several positive bio-effects of ultrasound and microbubble-induced BBB opening have been reported. In rodent models of Alzheimer's disease, numerous positive effects have been discovered in the absence of exogenous therapeutics. These effects include a reduction in amyloid-β plaque load (Jordão et al. 2013; Burgess et al. 2014; Leinenga and Götz 2015; Poon et al. 2018), reduction in tau pathology (Pandit et al. 2019) and improvements in spatial memory (Burgess et al. 2014; Leinenga and Götz 2015). Two-photon microscopy has revealed that amyloid-β plaque size is reduced in transgenic mice for up to 2 wk after ultrasound and microbubble treatment (Poon et al. 2018). Opening of the BBB in both transgenic and wild-type mice has also revealed enhanced neurogenesis (Burgess et al. 2014; Scarcelli et al. 2014; Mooney et al. 2016) in the treated tissue.

Gene delivery to the CNS using ultrasound and microbubbles is another area that is increasingly being investigated. Viral (Alonso et al. 2013; Wang et al. 2015b) and non-viral (Mead et al. 2016) delivery methods have been investigated. While early studies reported the feasibility of gene delivery using reporter genes (*e.g.,* Thevenot et al. 2012; Alonso et al. 2013), there have been promising results delivering therapeutic genes. In particular, advances have been made in Parkinson's disease models, where therapeutic genes have been tested (Mead et al. 2017; Xhima et al. 2018) and where long-lasting functional improvements have been reported in response to therapy (Mead et al. 2017). It is expected that research into this highly promising technique will expand to a range of therapeutic applications.

Despite excellent tolerability profiles in non-human primate studies investigating repeat opening of the BBB (McDannold et al. 2012; Downs et al. 2015), there has been recent controversy because of reports of a sterile inflammatory response observed in rats (Kovacs et al. 2017a, 2017b; Silburt et al. 2017). The inflammatory response is proportional to the magnitude of BBB opening and is therefore strongly influenced by experimental conditions such as microbubble dose and acoustic settings. However, McMahon and Hynynen (2017) reported that when clinical microbubble doses are used, and treatment exposures are actively controlled to avoid overtreating, the inflammatory response is acute and mild. They note that while chronic inflammation is undesirable, acute inflammation may actually contribute to some of the positive bio-effects that have been observed. For example, the clearance of amyloid-β after ultrasound and microbubble treatment is thought to be mediated in part by microglial activation (Jordão et al. 2013). These findings reiterate the need for carefully controlled treatment exposures to select for desired bio-effects.

Cavitation monitoring and control

It is generally accepted that the behavior of the microbubbles in the ultrasound field is predictive, to an extent, of the observed bio-effects. In the seminal study on the association between cavitation and BBB opening, McDannold et al. (2006) observed an increase in second harmonic emissions in cases of successful opening, compared with exposures that led to no observable changes in permeability as measured by contrast-enhanced MRI. Further, they noted that successful opening could be achieved in the absence of inertial cavitation, which was also reported by another group (Tung et al. 2010). These general guidelines have been central to the development of active treatment control schemes that have been developed to date—all with the common goal of promoting stable bubble oscillations, while avoiding violent bubble collapse that can lead to tissue damage. These methods are based either on detection of sub- or ultraharmonic (O'Reilly and Hynynen 2012; Tsai et al. 2016; Bing et al. 2018), harmonic bubble emissions (Arvanitis et al. 2012; Sun et al. 2017) or a combination thereof (Kamimura et al. 2019). An approach based on the sub-/ultraharmonic controller developed by O'Reilly and Hynynen (2012) has been employed in early clinical testing (Lipsman et al. 2018; Mainprize et al. 2019).

Control methods presented to date have generally been developed using single receiver elements, which simplifies data processing but does not allow signals to be localized. Focused receivers are spatially selective but can miss off-target events, while planar receivers may generate false positives based on signals originating outside the treatment volume. The solution to this is to use an array of receivers and passive beamforming methods, combined with phase correction methods to compensate for the skull bone (Jones et al. 2013, 2015), to generate maps of bubble activity. In the brain this has been achieved with linear arrays (Arvanitis et al. 2013; Yang et al. 2019c), which suffer from poor axial resolution when using passive imaging methods, as well as large-scale sparse hemispherical or large aperture receiver arrays (O'Reilly et al. 2014; Deng et al. 2016; Crake et al. 2018; Jones et al. 2018; Liu et al. 2018a) that optimize spatial resolution for a given frequency. Recently, this has extended beyond just imaging the bubble activity to incorporate real-time, active feedback control based on both the spectral and spatial information obtained from the bubble maps (Jones et al. 2018) (Fig. 4). Robust control methods building on these works will be essential for widespread adoption of this technology to ensure tolerable and consistent treatments.

BSCB opening

Despite the similarities between the BBB and BSCB, and the great potential benefit for patients, there has been limited work investigating translation of this technology to the spinal cord. Opening of the BSCB in rats was first reported by Wachsmuth et al. (2009), and was followed by studies from Weber-Adrien et al. (2015), Payne et al. (2017) and O'Reilly et al. (2018) in rats (Fig. 5) and from Montero et al. (2019) in rabbits, the latter performed through a laminectomy window. In 2018, O'Reilly et al. (2018) presented the first evidence of a therapeutic benefit in a disease model, showing improved tumor control in a rat model of leptomeningeal metastases.

Although promising, significant work remains to be done to advance BSCB opening to clinical studies. A more thorough characterization of the bio-effects in the spinal cord and how, if at all, they differ from those in the brain is necessary to ensure safe translation. Additionally, methods and devices capable of delivering controlled therapy to the spinal cord at clinical scale are needed. While laminectomy and implantation of an ultrasound device (Montero et al. 2019) might be an appropriate approach for some focal indications, treating multifocal or diffuse disease will require the ultrasound

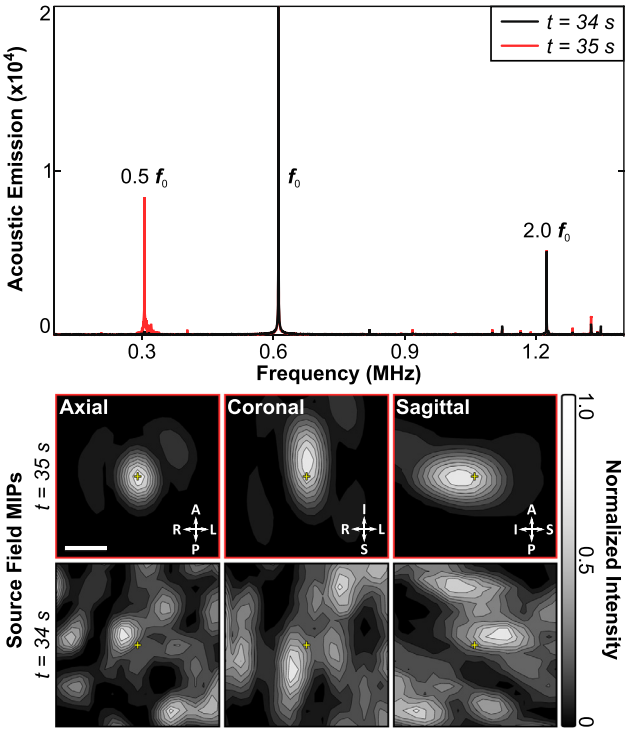

Fig. 4. Three-dimensional transcranial subharmonic microbubble imaging and treatment control *in vivo* in rabbit brain during blood–brain barrier opening. Spectral information (top) indicates the appearance of subharmonic activity at $t = 35$ s into the treatment. Passive mapping of the subharmonic band localizes this activity to the target region. Bar = 2.5 mm. Reprinted (adapted), with permission, from Jones et al. (2018).

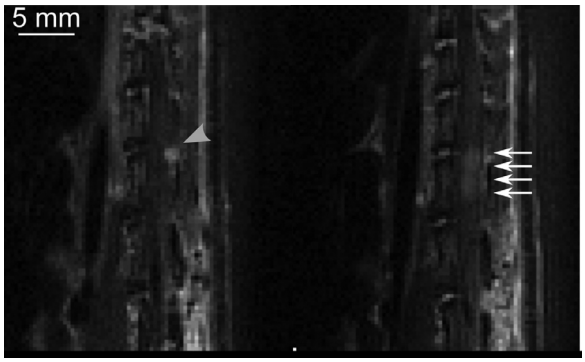

Fig. 5. T_1-Weighted sagittal magnetic resonance images revealing leptomeningeal tumors in rat spinal cord (*gray arrowhead*) before ultrasound and microbubble treatment (left column), and the enhancement of the cord indicating blood–spinal cord barrier opening (*white arrows*) after ultrasound and microbubble treatment (right column). Reprinted (adapted) with permission from O'Reilly et al. (2018).

to be delivered through the intact bone to the narrow spinal canal. Fletcher and O'Reilly (2018) have described a method to suppress standing waves in the human vertebral canal. Combined with devices suited to the spinal geometry, such as that presented by Xu and O'Reilly, (2020), these methods will help to advance clinical translation.

Clinical studies

The feasibility of enhancing BBB permeability in and around brain tumors using ultrasound and microbubbles has now been tested in two clinical trials. In the study conducted at Assistance Publique-Hôpitaux de Paris in Paris, France, an unfocused 1-MHz ultrasound transducer (SonoCloud) was surgically placed over the tumor resection area and permanently fixed into the hole in the skull bone. The skin was placed over the transducer, and after healing, treatments were conducted by inserting a needle probe through the skin to provide the driving signal to the transducer. Monthly treatments were then conducted while infusing a chemotherapeutic agent into the bloodstream (carboplatin). The sonication was executed during infusion of SonoVue microbubbles. A constant pulsed sonication was applied during each treatment, followed by a contrast-enhanced MRI to estimate BBB permeability. The power was escalated for each monthly treatment until enhancement was detected on MRI. This study reported the feasibility and tolerability (Carpentier et al. 2016), and a follow-up study may indicate increase in survival (Idbaih et al. 2019).

The second brain tumor study was conducted at Sunnybrook Health Sciences Centre in Toronto, Canada, which used the InSightec Exablate 220 kHz device and through-skull MRI-guided sonications of brain tumors before the surgical resection. It also described the feasibility of inducing highly localized BBB permeability enhancement and tolerability, and reported that chemotherapeutic concentration in the sonicated peritumor tissue was higher than in the unsonicated tissue (Mainprize et al. 2019).

Another study conducted in Alzheimer's disease patients with the Exablate device reported tolerable BBB permeability enhancement and that the treatment could be repeated 1 mo later without any imaging or behavior indications of adverse events (Lipsman et al. 2018). A third study with the same device investigated the feasibility of using functional MRI to target motor cortex in amyotrophic lateral sclerosis patients, again finding precisely targeted BBB permeability enhancement without adverse effects in this delicate structure (Abrahao et al. 2019). All of these studies were conducted using Definity microbubbles. These studies have led to the current ongoing brain tumor trial with six monthly treatments of the brain tissue surrounding the resection cavity during the maintenance phase of the treatment with temozolomide. This study sponsored by InSightec is being conducted in multiple institutions. Similarly, a phase II trial in Alzheimer's disease sonicating the hippocampus with the goal of investigating the tolerability and potential benefits from repeated (three treatments with 2-wk interval) BBB permeability enhancement alone is ongoing. This study is also being conducted in several institutions that have the device.

SONOTHROMBOLYSIS

Occlusion of blood flow through diseased vasculature is caused by thrombi, blood clots that form in the body. Because of limitations in thrombolytic efficacy and speed, sonothrombolysis, ultrasound which accelerates thrombus breakdown alone, or in combination with thrombolytic drugs and/or cavitation nuclei, has been under extensive investigation in the last two decades (Bader et al. 2016). Sonothrombolysis promotes thrombus dissolution for the treatment of stroke (Alexandrov et al. 2004a, 2004b; Molina et al. 2006; Chen et al. 2019), myocardial infarction (Mathias et al. 2016, 2019; Slikkerveer et al. 2019), acute peripheral arterial occlusion (Ebben et al. 2017), deep vein thrombosis (DVT) (Shi et al. 2018) and pulmonary embolism (Dumantepe et al. 2014; Engelberger and Kucher 2014; Lee et al. 2017).

Mechanisms, agents and approaches

Ultrasound improves recombinant tissue plasminogen activator (rt-PA) diffusion into thrombi and augments lysis primarily *via* acoustic radiation force and streaming (Datta et al. 2006; Prokop et al. 2007; Petit et al. 2015). Additionally, ultrasound increases rt-PA and plasminogen penetration into the thrombus surface

and enhances removal of fibrin degradation products *via* ultrasonic bubble activity, or acoustic cavitation, which induces microstreaming (Elder 1958; Datta et al. 2006; Sutton et al. 2013). Two types of cavitation are correlated with enhanced thrombolysis: stable cavitation, with highly non-linear bubble motion resulting in acoustic emissions at the subharmonic and ultraharmonics of the fundamental frequency (Flynn 1964; Phelps and Leighton 1997; Bader and Holland 2013), and inertial cavitation, with substantial radial bubble growth and rapid collapse generating broadband acoustic emissions (Carstensen and Flynn 1982; Flynn 1982).

Specialized contrast agents and tailored ultrasound schemes have been investigated with the aim of optimizing sonothrombolysis. Petit et al. (2015) observed a greater degree of rt-PA lysis with BR38 microbubbles exposed to 1 MHz pulsed ultrasound at an amplitude causing inertial cavitation (1.3 MPa peak rarefactional pressure) than at a lower amplitude causing stable cavitation (0.35 MPa peak rarefactional pressure). Goyal et al. (2017) also measured a higher degree of thrombolysis with 1 MHz pulsed ultrasound at 1.0 MPa peak rarefactional pressure with inertial cavitation than at 0.23 MPa peak rarefactional pressure with stable cavitation in an *in vitro* model of microvascular obstruction using perfluorobutane-filled, lipid-shelled microbubbles (Weller et al. 2002) as a nucleation agent. However, Kleven et al. (2019) observed more than 60% fractional clot width loss for highly retracted human whole blood clots exposed to rt-PA, Definity and 220 kHz pulsed or continuous wave (CW) ultrasound at an acoustic output with sustained stable cavitation throughout the insonification periods (0.22 MPa peak rarefactional pressure) (Fig. 6).

Echogenic liposomes loaded with rt-PA enhanced lysis compared with rt-PA alone at concentrations of 1.58 and 3.15 mg/mL (Shekhar et al. 2017), suggesting that encapsulation of rt-PA could reduce the rt-PA dose by a factor of 2 with equivalent lytic activity. Subsequently it has been found that these liposomes protect rt-PA against degradation by plasminogen activator inhibitor 1, while achieving equivalent thrombolytic efficacy relative to rt-PA, Definity and intermittent 220 kHz CW ultrasound (Shekhar et al. 2019). Promising agents, including a nanoscale (<100 nm) contrast agent (Brüssler et al. 2018) and magnetically targeted microbubbles (De Saint Victor et al. 2019), have also exhibited enhanced rt-PA thrombolysis *in vitro*. All of these investigators noted that in the absence of rt-PA, the combination of ultrasound and microbubbles did not degrade the fibrin network.

Several minimally invasive techniques have also been explored, with or without the inclusion of rt-PA or exogenous cavitation nuclei. In the clinical management of stroke, rapid treatments are needed because of the

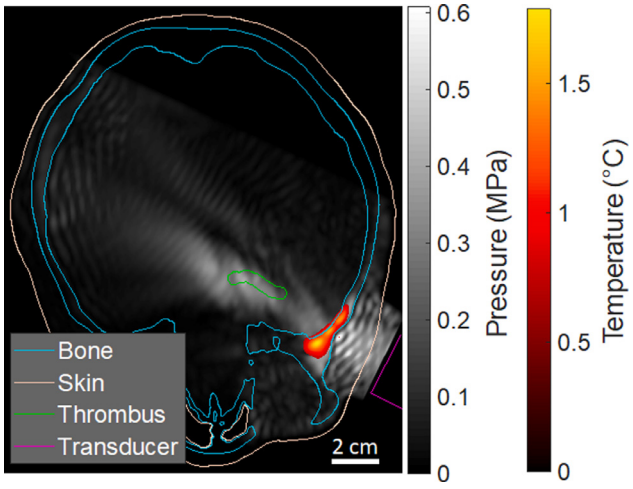

Fig. 6. Simulated acoustic pressure and temperature in a representative subject exposed to pulsed 220 kHz ultrasound with a 33.3% duty cycle. The absolute peak-to-peak pressure maximum for the simulations is displayed in gray scale. Temperature is displayed using a heat map with a minimum color priority write threshold of 1°C. Computed tomography features such as bone (*cyan*), skin and internal epithelium (*beige*) and clot (*green*) are plotted using contour lines. The transducer is outlined in *magenta*. Constructive interference is prominent in the soft tissue between the temporal bone and the transducer. Some constructive interference is also present in the brain tissue close to the contralateral temporal bone; however, the pressure in this region did not exceed the pressure in the M1 section of the middle cerebral artery. Temperature rise was prominent in the ipsilateral bone along the transducer axis. The computational model is described in Kleven et al. (2019).

neurologist's adage "time is brain." Thus, treatment options that promote fast clot removal, reduce edema and intracerebral bleeding and improve patient outcomes are of immense value. Magnetic resonance image-guided HIFU has been investigated for the treatment of both ischemic (Burgess et al. 2012) and hemorrhagic (Monteith et al. 2013) stroke, and Zafar et al. (2019) have provided an excellent review of the literature for this approach. Histotripsy, a form of HIFU that relies on the mechanical action of microbubble clouds to ablate thrombi with and without rt-PA (Maxwell et al. 2009; Bader et al. 2015, 2019; Zhang et al. 2016b) is under development to treat deep vein thrombosis. Additionally, ultrasound-accelerated catheter-directed thrombolysis using the EKOS system (EKOS/BTG, Bothell, WA, USA) combines 2 MHz low-intensity pulsed ultrasound and rt-PA without cavitation nuclei to improve lytic efficiency to treat DVT (Shi et al. 2018) and pulmonary embolism (Garcia 2015).

Cavitation monitoring

Acoustic cavitation has been reported to mediate direct fibrinolysis (Weiss et al. 2013) and accelerated rt-

PA lysis (Everbach and Francis 2000; Datta et al. 2006; Prokop et al. 2007; Hitchcock et al. 2011). Passive and active cavitation detection techniques have been developed to monitor acoustic cavitation (Roy et al. 1990; Madanshetty et al. 1991; Bader et al. 2015). Passive cavitation imaging, or passive acoustic mapping, employs a transducer array that listens passively (*i.e.,* no transmit) to emissions from acoustically activated microbubbles (Salgaonkar et al. 2009; Gyöngy and Coussios 2010; Haworth et al. 2017). Vignon et al. (2013) developed a prototype array enabling spectral analysis of bubble activity for sonothrombolysis applications. Superharmonic Doppler effects have also been utilized to monitor bubble activity from 500 kHz pulsed therapeutic ultrasound (Pouliopoulos and Choi 2016). Both a linear array (Arvanitis and McDannold 2013a, 2013b; Arvanitis et al. 2013) and a sparse hemispherical array (Acconcia et al. 2017) have been integrated into a clinical magnetic resonance image-guided HIFU system to assess microbubble dynamics during sonothrombolysis in the brain.

Pre-clinical studies

Information gathered from animal studies can help inform human clinical trials, despite a strong species dependence of clot rt-PA lytic susceptibility (Gabriel et al. 1992; Flight et al. 2006; Huang et al. 2017). A comprehensive systematic evaluation of 16 *in vivo* pre-clinical sonothrombolysis studies was carried out by Auboire et al. (2018) summarizing treatment efficacy and tolerability outcomes in models of ischemic stroke. Since that review was published, the efficacy of sonothrombolysis using nitrogen microbubbles stabilized with a non-cross-linked shell delivered intra-arterially through a catheter and rt-PA delivered intravenously has been explored in a rat model of ischemic stroke (Dixon et al. 2019).

Clinical studies

There exists a rich literature on clinical trials exploring the tolerability and efficacy of sonothrombolysis. Two recent meta-analyses of seven randomly assigned controlled trials (Chen et al. 2019; Zafar et al. 2019) attempt to determine whether the administration of rt-PA and ultrasound improves outcomes in acute ischemic stroke. Both analyses conclude that sonothrombolysis significantly enhances complete or partial recanalization, with improved neurologic function (assessed *via* the National Institutes of Health Stroke Scale). An ongoing clinical trial (Aureva Transcranial Ultrasound Device With tPA in Patients With Acute Ischemic Stroke (TRUST), NCT03519737) will determine whether large vessel occlusions can be re-canalized with sonothrombolysis (Cerevast Medical, Inc., Bothell, WA, USA) and rt-PA, tenecteplase or alteplase (Campbell et al. 2018), while patients are transferred to a stroke center for mechanical thrombectomy (Gauberti 2019).

Several clinical trials have indicated that high-MI pulsed diagnostic ultrasound exposure of Definity before and after percutaneous coronary intervention for ST elevation myocardial infarction can prevent microvascular obstruction and improve functional outcomes (Mathias et al. 2016, 2019; Slikkerveer et al. 2019). A systematic review of 16 catheter-directed sonothrombolysis clinical trials composed mostly of retrospective case series using the EKOS system without microbubble infusions determined that this treatment modality is tolerable and promising for the treatment of DVT (Shi et al. 2018). However, a large-sample randomly assigned prospective clinical trial is needed to improve the clinical evidence for use as a front-line therapy for DVT. In retrospective studies in patients with pulmonary embolism, Lee et al. (2017) conclude that catheter-directed sonothrombolysis is tolerable and decreases right-sided heart strain, but Schissler et al. (2018) conclude that this therapy is not associated with a reduction in mortality or increased resolution of right ventricular dysfunction. And finally, an ongoing trial in a small cohort of 20 patients with acute peripheral arterial occlusions (Ebben et al. 2017) will determine whether Luminity (marketed in the United States as Definity) and 1.8 MHz transdermal diagnostic ultrasound with intermittent high MI (1.08) and low MI (0.11) for visualization of the microbubbles and flow will improve recanalization. In summary, sonothrombolysis has been found to have clinical benefit in the treatment of acute and chronic thrombotic disease. Ultrasound-assisted thrombolysis has a potential role as an emerging viable and therapeutic option for future management of stroke and cardiovascular disease.

CARDIOVASCULAR DRUG DELIVERY AND THERAPY

In cardiovascular drug delivery, cavitation nuclei are co-administered or loaded with different therapeutics for the treatment of various diseases. For atherosclerosis treatment in an ApoE-deficient mouse model, intercellular adhesion molecule-1-targeted microbubbles carrying the angiogenesis inhibitor Endostar were used (Yuan et al. 2018). Upon intermittent insonification over the abdominal and thoracic cavity with 1 MHz ultrasound (2 W/cm^2 intensity, 50% duty cycle) for 30 s with two repeats and another treatment 48 h later, plaque area and intraplaque neovascularization were significantly reduced 2 wk after treatment. Percutaneous coronary intervention is often used to restore blood flow in atherosclerotic arteries. The treatment of coronary microembolization, a complication of percutaneous coronary intervention, was demonstrated in pigs treated with ultrasound (1 MHz, 2.0 W/cm^2 intensity, 10 s on and 10 s off,

20-min duration) and microRNA-21-loaded microbubbles 4 d before coronary microembolization (Su et al. 2015). This resulted in an improved cardiac dysfunction. Although not a therapeutic study, Liu et al. (2015) did find that plasmid transfection to the myocardium was significantly larger when the microbubbles were administered into the coronary artery compared with intravenously *via* the ear vein in pigs even though the intracoronary microbubble dose was half of the intravenous dose (1 MHz ultrasound, 2 W/cm^2, 50% duty cycle, 20-min duration). Percutaneous coronary intervention can also result in neointimal formation, which induces restenosis. Sirolimus-loaded microbubbles were found to reduce neointimal formation in coronary arteries by 50% in pigs (see Fig. 7), 28 d after angioplasty in combination with a mechanically rotating intravascular ultrasound catheter (5 MHz, 500 cycles, 50% duty cycle, 0.6-MPa peak negative pressure) (Kilroy et al. 2015). Another research group reported that paclitaxel-loaded microbubbles and ultrasound (1 MHz, 1.5 MPa for 10 s) can also significantly inhibit neointimal formation in the iliac artery in rabbits 1 wk after percutaneous coronary intervention (Zhu et al. 2016).

In diabetic cardiomyopathy, microbubble-mediated delivery of fibroblast growth factor has shown therapeutic effects. Zhao et al. (2016) could prevent diabetic cardiomyopathy in rats by treating the heart with ultrasound (14 MHz, 7.1 MPa for 10 s, three repeats with off interval of 1 s) and microbubbles co-administered with acidic fibroblast growth factor nanoparticles twice weekly for 12 consecutive wk. In already established diabetic cardiomyopathy in rats, the same investigators co-administered basic fibroblast growth factor-containing nanoparticles with microbubbles with the same ultrasound treatment, albeit that it was given three times with 1 d in between treatments. At 4 wk after treatment, this resulted in restored cardiac function as a result of structural remodeling of the cardiac tissue (Zhao et al. 2014). Microbubbles loaded with acidic fibroblast growth factor in combination with ultrasound (14 MHz, 7.1 MPa for 10 s, three repeats with off interval of 1 s) also resulted in significantly improved cardiac function in a rat model of diabetic cardiomyopathy. Treatment was performed twice weekly for 12 consecutive wk (Zhang et al. 2016a). For doxorubicin-induced cardiomyopathy, repeated co-administration of microbubbles and nanoparticles containing acidic fibroblast growth factor in combination with ultrasound (14 MHz, 7.1 MPa for 10 s, three repeats with off interval of 1 s) applied at the heart successfully prevented doxorubicin-induced cardiomyopathy in rats (Tian et al. 2017). Once doxorubicin-induced cardiomyopathy had occurred, microbubble-mediated reversal of cardiomyopathy was shown by the delivery of surviving plasmid to cardiomyocytes and endothelial cells (Lee et al. 2014) or glucagon-like peptide-1 to cardiomyocytes, endothelial cells, vascular muscle cells and mesenchymal cells (Chen et al. 2015) in rats. The ultrasound settings were 5 MHz (120 V power, pulsing interval of 10 cardiac cycles at end-systole) for a 5 min treatment (Lee et al. 2014) or not specified (Chen et al. 2015). The microbubble-mediated gene therapy study by Chen et al. (2016) indicated that ANGPTL8 gene therapy does not need to be done in the heart to reverse doxorubicin-induced cardiomyopathy in rats as their microbubble and ultrasound (1.3 MHz, 1.4 MPa peak negative pressure, four bursts triggered to every fourth end-systole using a delay of 45−70 ms of the peak of the R wave) therapy was done in the liver (90 s treatment). This resulted in overexpression of ANGPTL8 in liver cells and blood, which stimulated cardiac progenitor cells in the epicardium.

A few dozen articles have been published on treating myocardial infarction with microbubble and ultrasound-mediated gene delivery *in vivo*, in mouse, rat, rabbit and dog models. These are reviewed by Qian et al. (2018). Amongst these are a few targeted microbubble studies which all indicate that the targeted microbubbles induced higher degrees of gene transfection, increased myocardial vascular density and improved cardiac function in comparison to non-targeted microbubbles. This improvement occurred independent of the type of ligand on the microbubble, the gene that was transfected or the animal model: matrix metalloproteinase 2 target with Timp3 gene in rats (Yan et al. 2014), intracellular adhesion molecule-1 target with Ang-1 gene in rabbits (Deng et al. 2015), P-selectin target with hVEGF165 gene in rats (Shentu et al. 2018). Ultrasound settings for these studies were similar at 1.6 MHz (1.6 MPa peak negative pressure, pulsing interval of 4 cardiac cycles) for 20 min during infusion of the plasmid-loaded microbubbles (both Yan et al. [2014] and Shentu et al. [2018]) or 1.7 MHz (1.7 MPa peak negative pressure, pulsing interval every 4−8 cardiac cycles) for 5 min after bolus injection of the plasmid-loaded microbubbles (Deng et al. 2015).

Other gene therapy studies for vascular disease include stimulating angiogenesis for the treatment of chronic hindlimb ischemia in rats using miR-126-3p-loaded microbubbles and ultrasound (1.3 MHz, 2.1 MPa peak negative acoustic pressure, pulsing interval 5 s). The treatment lasted 20 min during which microbubbles were infused for 10 min and resulted in improved perfusion, vessel density, arteriolar formation and neovessel maturation (Cao et al. 2015). Recently, successful gene therapy was reported in baboons in which vascular endothelial growth factor (VEGF)-plasmid loaded microbubbles were infused and ultrasound (2−6 MHz, MI 1.9, repeated 5 s burst pulses with three bursts per min) was applied for 10 min on days 25, 35, 45 and 55 of

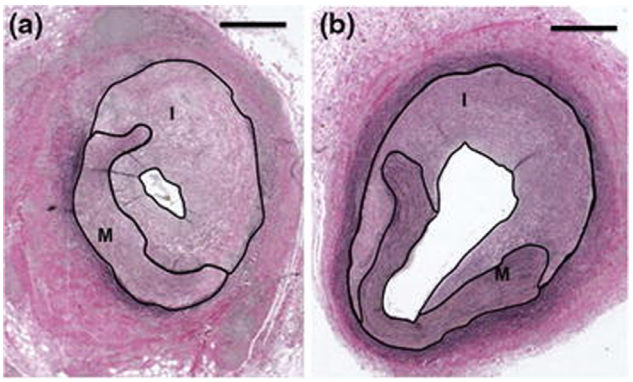

Fig. 7. Histologic sections of a coronary artery of a pig 28 d after angioplasty. Pigs were treated with sirolimus-loaded microbubbles only (a) or sirolimus-loaded microbubbles and ultrasound (b) using a mechanically rotating intravascular ultrasound catheter (5 MHz, 500 cycles, 50% duty cycle, 0.6 MPa peak negative pressure). Treatment with ultrasound and sirolimus-loaded microbubbles reduced neointimal formation by 50%. In both sections, the intima (I) and media (M) are outlined. Bar = 500 μm. Reprinted with permission from Springer Nature: Springer, Annals of Biomedical Engineering, Reducing Neointima Formation in a Swine Model with IVUS and Sirolimus Microbubbles, Kilroy JP, Dhanaliwala AH, Klibanov AL, Bowles DK, Wamhoff BR, Hossack JA, COPYRIGHT, from Kilroy JP et al. (2015).

gestation, with the transducer placed over the placental basal plate (Babischkin et al. 2019). This was a mechanistic study elucidating the role of VEGF in uterine artery remodeling.

The gas core of the cavitation nuclei can also be the therapeutic. Sutton et al. (2014) have found that ultrasound-mediated (1 MHz, 0.34 MPa acoustic pressure, 30 cycle pulse, 50 s treatment) nitric oxide gas delivery from echogenic liposomes to *ex vivo*-perfused porcine carotid arteries induces potent vasorelaxation. The vasodilative effect of nitric oxide-loaded echogenic liposomes upon insonification (5.7 MHz, 0.36 MPa peak negative pressure, 30 s treatment) was also shown in *ex vivo* perfused rabbit carotid arteries with arterial wall penetration of nitric oxide confirmed by fluorescence microscopy (Kim et al. 2014). In addition to this, vasodilative effects were reported in carotid arteries *in vivo* in rats with vasospasms after subarachnoid hemorrhage using 1 MHz ultrasound with 0.3 MPa peak-to-peak pressure, 50% duty cycle for a duration of 40 min with constant infusion of the echogenic liposomes. This resulted in improved neurologic function (limb placement, beam and grid walking) (Kim et al. 2014). Ultrasound activation of the antioxidant hydrogen gas encapsulated in microbubbles was reported to prevent myocardial ischemia–reperfusion injury in rats when administered before reperfusion (He et al. 2017). There was a dose-dependent effect as 2×10^{10} microbubbles resulted in a more significant reduction in infarct size (70%) than 4×10^{9} microbubbles (39%) compared with vehicle-treated rats. Furthermore, treatment with the high-dose hydrogen microbubbles prevented changes in left ventricular end-diastolic and left ventricular end-systolic dimensions, as well as minimal reductions in ejection fraction and fractional shortening. Histologic and ELISA analyses revealed a reduced degree of myocardial necrosis, apoptosis, hemorrhaging, inflammation and oxidant damage. At the same time that cardiovascular drug delivery and therapy using microbubbles and ultrasound is moving forward to large animal and clinical studies, sophisticated *in vitro* models are being used and/or developed for mechanistic studies, such as flow chambers (μSlides, Ibidi) (Shamout et al. 2015) and perfused 3-D microvascular networks (Juang et al. 2019), in which human umbilical vein endothelial cells are grown.

Clinical study

Microbubbles and ultrasound were clinically investigated to augment muscle blood flow in 12 patients with stable sickle cell disease in the absence of a drug at the Oregon Health & Science University, Portland, Oregon, USA (Belcik et al. 2017). Perfusion increased ~2-fold in the forearm flexor muscles upon Definity infusion and insonification at 1.3 MHz (MI 1.3). Ultrasound was applied three times for 3 min with ~5 min intervals. The change in perfusion was determined from contrast-enhanced ultrasound imaging and extended well beyond the region where ultrasound was applied. This study indicated that the therapeutic ultrasound settings directly translate from mouse to human for superficial muscles, as the same investigators found augmented blood flow in ischemic and non-ischemic hindlimb muscles in mice in the same study and an earlier publication (Belcik et al. 2015). However, for the pre-clinical studies, custom-made microbubbles were used instead of Definity.

SONOBACTERICIDE

Sonobactericide has been defined as the use of ultrasound in the presence of cavitation nuclei for the enhancement of bactericidal action (Lattwein et al. 2018). This topic has recently gained attention, with 17 papers being published in the last 5 y. Research on ultrasound-mediated enhancement of antimicrobials has focused on several sources of infections including general medical devices (Ronan et al. 2016; Dong et al. 2017, 2018; Hu et al. 2018; Fu et al. 2019), acne (Liao et al. 2017), chronic bacterial prostatitis (Yi et al. 2016), infective endocarditis (Lattwein et al. 2018), pneumonia (Sugiyama et al. 2018), prosthetic joint infections (Li et al. 2015; Lin et al. 2015; Guo et al. 2017a; Zhou et al. 2018) and urinary tract

infections (Horsley et al. 2019). However, there was no specific disease aim in two studies (Zhu et al. 2014; Goh et al. 2015). One group targeted membrane biofouling for water and wastewater industries (Agarwal et al. 2014). Direct bacterial killing, biofilm degradation and dispersal and increased or synergistic therapeutic effectiveness of antimicrobials have been reported as the therapeutic effects of sonobactericide. These studies show that sonobactericide can be applied to treat Gram+ or Gram− bacteria, when they are planktonic, associated with a surface and embedded in biofilm, or intracellular. The majority of these studies were carried out *in vitro*. However, seven were performed *in vivo* in either mice (Li et al. 2015; Liao et al. 2017; Sugiyama et al. 2018; Zhou et al. 2018), rats (Yi et al. 2016) or rabbits (Lin et al. 2015; Dong et al. 2018). Sonobactericide was mostly performed with co-administration of antimicrobials. Investigators also employed an antimicrobial encapsulated in liposomes that were conjugated to the microbubbles (Horsley et al. 2019), or the antimicrobial lysozyme was a microbubble coating (Liao et al. 2017) or did not use antimicrobials altogether (Agarwal et al. 2014; Goh et al. 2015; Yi et al. 2016). An extensive review of sonobactericide has been published recently by Lattwein et al. (2020). Although sonobactericide is an emerging strategy to treat bacterial infections with intriguing potential, the mechanism and safety of the treatment should be explored, particularly with respect to biofilm degradation and dispersal. Future studies should also focus on maximizing the efficacy of sonobactericide *in situ*.

FUTURE PERSPECTIVES AND CONCLUSIONS

Therapeutic ultrasound technology is experiencing a paradigm shift in terms of both technical developments and clinical applications. In addition to its inherent advantages for imaging (*e.g.,* real-time nature, portability and low cost), ultrasound in combination with cavitation nuclei is under exploration as a drug delivery modality. The results from several pre-clinical studies have already illustrated the potential of ultrasound-responsive cavitation nuclei to deliver multiple types of drugs (including model drugs, anticancer drugs, therapeutic antibodies, genes and nanoparticles) efficiently in various tumor models, including both ectopic and orthotopic models, for immunotherapy, brain disease, dissolution of clots and treatment of cardiovascular disease and bacterial infections.

Based on these encouraging pre-clinical data, several clinical trials have been initiated and others are planned. However, whilst animal studies provide proof of concept and impetus for clinical studies, careful attention must be given to their relevance in human disease, in particular, the applicability of therapeutic protocols and appropriate ultrasound settings. Otherwise we risk underestimating the therapeutic effects and potential deleterious side effects. The elucidation of all of the interactions between cavitation nuclei, cells and drugs will help to address this need. The biggest challenges lie in the large differences in time scales between the cavitation initiation, drug

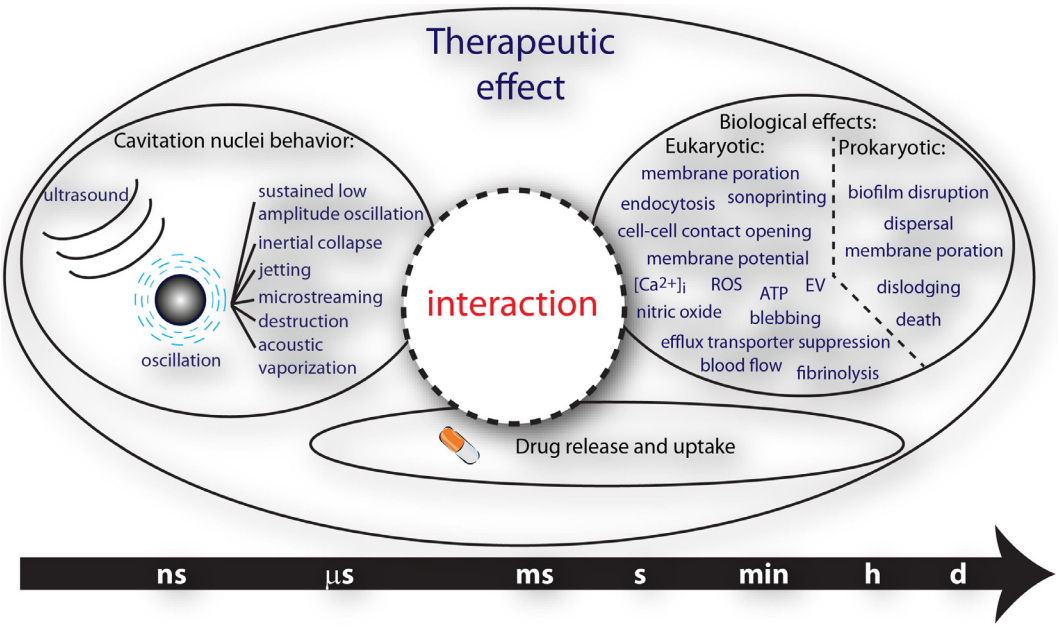

Fig. 8. Different time scales of the therapeutic effects of ultrasound and cavitation nuclei treatment. $[Ca^{2+}]_i$ = intracellular calcium; ROS = reactive oxygen species; ATP = adenosine triphosphate; EV = extracellular vesicles. Reprinted (adapted) with permission from Lattwein et al. (2020).

release and uptake and a biological response (Fig. 8). A multidisciplinary approach is needed to tackle these challenges integrating expertise in physics, biophysics, biology, chemistry and pharmacology.

Custom-made microbubbles which serve as cavitation nuclei are often used for ultrasound-mediated drug delivery studies. An advantage is full control over the payload, as well as the disease target. At the same time, full acoustical characterization and sterility of the microbubbles must be considered during translation to human studies, which often requires approval from the U.S. Food and Drug Administration (FDA) or other similar federal agencies in Europe and Asia. As an example, for gene therapy, will each different type of genetic material loaded onto microbubbles need such approval, or will a class of cationic microbubbles be approved regardless of the specific gene? The former path would hinder fast clinical translation. For now, co-administration of drugs with FDA-approved ultrasound contrast agents is being explored in clinical trials. Apart from applications in the brain, ongoing clinical studies evaluating microbubble-mediated drug delivery are based on standard clinical ultrasound scanners operating mostly in Doppler mode. To promote the progress of this emerging technology, it is very important to design and implement specific therapeutic ultrasound pulse sequences that might be vastly different from clinical diagnostic imaging output. Clinical scanners can indeed be modified to be able to generate drug delivery protocols. In a similar way that elastography requires long ultrasound pulses to generate the push sequences (Deffieux et al. 2009), ultrasound scanners can be modified to be able to transmit drug delivery ultrasound sequences with tailored and optimized parameters (pulse duration, duty cycle and center frequency).

Ultimately, ultrasound image-guided drug delivery and the monitoring of treatment response could be feasible with the same equipment. Additionally, with recent developments in ultrasound imaging technology, ultrasound-mediated therapy could be planned, applied and monitored in a rapid sequence with high spatial and temporal resolution. The use of a single imaging and therapy device would alleviate the need for co-registration, because the imaging equipment would also be used to induce localized therapy ensuring a perfect co-location. Nonetheless, a compromise between efficacy and safety remains a major challenge for successful clinical applications of this dual methodology, which combines real-time image guidance of therapeutic delivery.

In conclusion, ultrasound-responsive microbubbles which serve as cavitation nuclei are being used to treat a wide variety of diseases and show great potential preclinically and clinically. The elucidation of the cavitation nuclei−cell interaction and the implementation of drug delivery ultrasound sequences on clinical ultrasound scanners are expected to invigorate clinical studies.

Acknowledgments—Financial support from the European Research Council under the European Union's Horizon 2020 research and innovation programme (Grant Agreement No 805308, PI: K.K.); Phospholipid Research Center in Heidelberg, Germany (PhD grant, PI: K.K.); FWO Vlaanderen (Grant 12E3916N); U.S. Department of Health and Human Services, National Institutes of Health, National Institute of Neurological Disorders and Stroke (Grant R01 NS047603, PI: C.K.H.; Grant R01 HL135092 and Grant R01 HL133334, PI of subK: C.K.H.); Engineering and Physical Sciences Research Council (Grants EP/I021795/1 and EP/L024012/1, PI: E.S.); and Canada Research Chair Program (PI: K.H., PI: M.A.O.) is gratefully acknowledged.

Conflict of interest disclosure—The authors declare no conflict of interest.

REFERENCES

Abrahao A, Meng Y, Llinas M, Huang Y, Hamani C, Mainprize T, Aubert I, Heyn C, Black SE, Hynynen K, Lipsman N, Zinman L. Motor cortex blood-brain barrier opening in amyotrophic lateral sclerosis using MR-guided focused ultrasound: A first-in-human trial. Nat Commun 2019;10:4373.

Acconcia CN, Leung BY, Goertz DE. The microscale evolution of the erosion front of blood clots exposed to ultrasound stimulated microbubbles. J Acoust Soc Am 2016;139:EL135.

Acconcia CN, Jones RM, Goertz DE, O'Reilly MA, Hynynen K. Megahertz rate, volumetric imaging of bubble clouds in sonothrombolysis using a sparse hemispherical receiver array. Phys Med Biol 2017;62:L31–L40.

Agarwal A, Jern Ng W, Liu Y. Removal of biofilms by intermittent low-intensity ultrasonication triggered bursting of microbubbles. Biofouling 2014;30:359–365.

Alexandrov AV, Demchuk AM, Burgin WS, Robinson DJ, Grotta JC, Investigators C. Ultrasound-enhanced thrombolysis for acute ischemic stroke: Phase I. Findings of the CLOTBUST trial. J Neuroimaging 2004;14:113–117.

Alexandrov AV, Wojner AW, Grotta JC, Investigators C. CLOTBUST: Design of a randomized trial of ultrasound-enhanced thrombolysis for acute ischemic stroke. J Neuroimaging 2004;14:108–112.

Alkins R, Burgess A, Ganguly M, Francia G, Kerbel R, Wels WS, Hynynen K. Focused ultrasound delivers targeted immune cells to metastatic brain tumors. Cancer Res 2013;73:1892–1899.

Alkins R, Burgess A, Kerbel R, Wels WS, Hynynen K. Early treatment of HER2-amplified brain tumors with targeted NK-92 cells and focused ultrasound improves survival. Neuro Oncol 2016;18:974–981.

Alonso A, Reinz E, Leuchs B, Kleinschmidt J, Fatar M, Geers B, Lentacker I, Hennerici MG, de Smedt SC, Meairs S. Focal delivery of AAV2/1-transgenes into the rat brain by localized ultrasound-induced BBB opening. Mol Ther Nucleic Acids 2013;2:e73.

Arvanitis C, McDannold N. Transcranial spatial and temporal assessment of microbubble dynamics for brain therapies. Proc Meet Acoust 2013;19 e075021.

Arvanitis CD, McDannold N. Integrated ultrasound and magnetic resonance imaging for simultaneous temperature and cavitation monitoring during focused ultrasound therapies. Med Phys 2013;40 112901.

Arvanitis CD, Livingstone MS, Vykhodtseva N, McDannold N. Controlled ultrasound-induced blood-brain barrier disruption using passive acoustic emissions monitoring. PLoS One 2012;7:e45783.

Arvanitis CD, Livingstone MS, McDannold N. Combined ultrasound and MR imaging to guide focused ultrasound therapies in the brain. Phys Med Biol 2013;58:4749–4761.

Aryal M, Vykhodtseva N, Zhang YZ, Park J, McDannold N. Multiple treatments with liposomal doxorubicin and ultrasound-induced

disruption of blood-tumor and blood-brain barriers improve outcomes in a rat glioma model. J Control Release 2013;169:103–111.
Aryal M, Fischer K, Gentile C, Gitto S, Zhang YZ, McDannold N. Effects on P-glycoprotein expression after blood-brain barrier disruption using focused ultrasound and microbubbles. PLoS One 2017;12 e0166061.
Auboire L, Sennoga CA, Hyvelin JM, Ossant F, Escoffre JM, Tranquart F, Bouakaz A. Microbubbles combined with ultrasound therapy in ischemic stroke: A systematic review of in-vivo preclinical studies. PLoS One 2018;13(2) e0191788.
Babischkin JS, Aberdeen GW, Lindner JR, Bonagura TW, Pepe GJ, Albrecht ED. Vascular endothelial growth factor delivery to placental basal plate promotes uterine artery remodeling in the primate. Endocrinology 2019;160:1492–1505.
Bader KB, Holland CK. Gauging the likelihood of stable cavitation from ultrasound contrast agents. Phys Med Biol 2013;58:127–144.
Bader KB, Gruber MJ, Holland CK. Shaken and stirred: Mechanisms of ultrasound-enhanced thrombolysis. Ultrasound Med Biol 2015;41:187–196.
Bader KB, Haworth KJ, Shekhar H, Maxwell AD, Peng T, McPherson DD, Holland CK. Efficacy of histotripsy combined with rt-PA in vitro. Phys Med Biol 2016;61:5253–5274.
Bader KB, Vlaisavljevich E, Maxwell AD. For whom the bubble grows: Physical principles of bubble nucleation and dynamics in histotripsy ultrasound therapy. Ultrasound Med Biol 2019;45:1056–1080.
Bae YJ, Yoon YI, Yoon TJ, Lee HJ. Ultrasound-guided delivery of siRNA and a chemotherapeutic drug by using microbubble complexes: In vitro and in vivo evaluations in a prostate cancer model. Korean J Radiol 2016;17:497–508.
Bao S, Thrall BD, Miller DL. Transfection of a reporter plasmid into cultured cells by sonoporation in vitro. Ultrasound Med Biol 1997;23:953–959.
Barenholz Y. Doxil—The first FDA-approved nano-drug: Lessons learned. J Control Release 2012;160:117–134.
Beekers I, van Rooij T, Verweij MD, Versluis M, de Jong N, Trietsch SJ, Kooiman K. Acoustic characterization of a vessel-on-a-chip microfluidic system for ultrasound-mediated drug delivery. IEEE Trans Ultrason Ferroelectr Freq Control 2018;65:570–581.
Beguin E, Shrivastava S, Dezhkunov NV, McHale AP, Callan JF, Stride E. Direct evidence of multibubble sonoluminescence using therapeutic ultrasound and microbubbles. ACS Appl Mater Interfaces 2019;11:19913–19919.
Belcik JT, Mott BH, Xie A, Zhao Y, Kim S, Lindner NJ, Ammi A, Linden JM, Lindner JR. Augmentation of limb perfusion and reversal of tissue ischemia produced by ultrasound-mediated microbubble cavitation. Circ Cardiovasc Imaging 2015;8(4) e002979.
Belcik JT, Davidson BP, Xie A, Wu MD, Yadava M, Qi Y, Liang S, Chon CR, Ammi AY, Field J, Harmann L, Chilian WM, Linden J, Lindner JR. Augmentation of muscle blood flow by ultrasound cavitation is mediated by ATP and purinergic signaling. Circulation 2017;135:1240–1252.
Benjamin TB, Ellis AT. The collapse of cavitation bubbles and the pressures thereby produced against solid boundaries. Phil Trans R Soc A 1966;260:221–240.
Bing C, Hong Y, Hernandez C, Rich M, Cheng B, Munaweera I, Szczepanski D, Xi Y, Bolding M, Exner A, Chopra R. Characterization of different bubble formulations for blood-brain barrier opening using a focused ultrasound system with acoustic feedback control. Sci Rep 2018;8:7986.
Bioley G, Lassus A, Terrettaz J, Tranquart F, Corthesy B. Long-term persistence of immunity induced by OVA-coupled gas-filled microbubble vaccination partially protects mice against infection by OVA-expressing Listeria. Biomaterials 2015;57:153–160.
Biro GP, Blais P. Perfluorocarbon blood substitutes. Crit Rev Oncol Hematol 1987;6:311–374.
Brüssler J, Strehlow B, Becker A, Schubert R, Schummelfeder J, Nimsky C, Bakowsky U. Nanoscaled ultrasound contrast agents for enhanced sonothrombolysis. Colloid Surface B 2018;172:728–733.
Bulner S, Prodeus A, Gariepy J, Hynynen K, Goertz DE. Enhancing checkpoint inhibitor therapy with ultrasound stimulated microbubbles. Ultrasound Med Biol 2019;45:500–512.
Burgess MT, Porter TM. Control of acoustic cavitation for efficient sonoporation with phase-shift nanoemulsions. Ultrasound Med Biol 2019;45:846–858.
Burgess A, Huang YX, Waspe AC, Ganguly M, Goertz DE, Hynynen K. High-intensity focused ultrasound (HIFU) for dissolution of clots in a rabbit model of embolic stroke. PLoS One 2012;7(8):e42311.
Burgess A, Dubey S, Yeung S, Hough O, Eterman N, Aubert I, Hynynen K. Alzheimer disease in a mouse model: MR imaging-guided focused ultrasound targeted to the hippocampus opens the blood-brain barrier and improves pathologic abnormalities and behavior. Radiology 2014;273:736–745.
Burke CW, Alexander E, Timbie K, Kilbanov AL, Price RJ. Ultrasound-activated agents comprised of 5 FU-bearing nanoparticles bonded to microbubbles inhibit solid tumor growth and improve survival. Mol Ther 2014;22:321–328.
Campbell BCV, Mitchell PJ, Churilov L, Yassi N, Kleinig TJ, Dowling RJ, Yan B, Bush SJ, Dewey HM, Thijs V, Scroop R, Simpson M, Brooks M, Asadi H, Wu TY, Shah DG, Wijeratne T, Ang T, Miteff F, Levi CR, Rodrigues E, Zhao H, Salvaris P, Garcia-Esperon C, Bailey P, Rice H, de Villiers L, Brown H, Redmond K, Leggett D, Fink JN, Collecutt W, Wong AA, Muller C, Coulthard A, Mitchell K, Clouston J, Mahady K, Field D, Ma H, Phan TG, Chong W, Chandra RV, Slater LA, Krause M, Harrington TJ, Faulder KC, Steinfort BS, Bladin CF, Sharma G, Desmond PM, Parsons MW, Donnan GA, Davis SM, for the EXTEND-IA TNK Investigators. Tenecteplase versus alteplase before thrombectomy for ischemic stroke. N Engl J Med 2018;378:1573–1582.
Cao WJ, Rosenblat JD, Roth NC, Kuliszewski MA, Matkar PN, Rudenko D, Liao C, Lee PJ, Leong-Poi H. Therapeutic angiogenesis by ultrasound-mediated microRNA-126-3p delivery. Arterioscler Thromb Vasc Biol 2015;35:2401–2411.
Cao Y, Chen Y, Yu T, Guo Y, Liu F, Yao Y, Li P, Wang D, Wang Z, Chen Y, Ran H. Drug release from phase-changeable nanodroplets triggered by low-intensity focused ultrasound. Theranostics 2018;8:1327–1339.
Carpentier A, Canney M, Vignot A, Reina V, Beccaria K, Horodyckid C, Karachi C, Leclercq D, Lafon C, Chapelon JY, Capelle L, Cornu P, Sanson M, Hoang-Xuan K, Delattre JY, Idbaih A. Clinical trial of blood-brain barrier disruption by pulsed ultrasound. Sci Transl Med 2016;8:343.re2.
Carstensen EL, Flynn HG. The potential for transient cavitation with microsecond pulses of ultrasound. Ultrasound Med Biol 1982;8:L720–L724.
Caskey CF, Qin S, Dayton PA, Ferrara KW. Microbubble tunneling in gel phantoms. J Acoust Soc Am 2009;125:EL183–EL189.
Chen PY, Liu HL, Hua MY, Yang HW, Huang CY, Chu PC, Lyu LA, Tseng IC, Feng LY, Tsai HC, Chen SM, Lu YJ, Wang JJ, Yen TC, Ma YH, Wu T, Chen JP, Chuang JI, Shin JW, Hsueh C, Wei KC. Novel magnetic/ultrasound focusing system enhances nanoparticle drug delivery for glioma treatment. Neuro Oncol 2010;12:1050–1060.
Chen H, Brayman AA, Kreider W, Bailey MR, Matula TJ. Observations of translation and jetting of ultrasound-activated microbubbles in mesenteric microvessels. Ultrasound Med Biol 2011;37:2139–2148.
Chen X, Leow RS, Hu Y, Wan JM, Yu AC. Single-site sonoporation disrupts actin cytoskeleton organization. J R Soc Interface 2014;11 20140071.
Chen S, Chen J, Huang P, Meng XL, Clayton S, Shen JS, Grayburn PA. Myocardial regeneration in adriamycin cardiomyopathy by nuclear expression of GLP1 using ultrasound targeted microbubble destruction. Biochem Biophys Res Commun 2015;458:823–829.
Chen S, Chen J, Meng XL, Shen JS, Huang J, Huang P, Pu Z, McNeill NH, Grayburn PA. ANGPTL8 reverses established adriamycin cardiomyopathy by stimulating adult cardiac progenitor cells. Oncotarget 2016;7:80391–80403.
Chen ZQ, Xue T, Huang HC, Xu JY, Shankar S, Yu H, Wang Z. Efficacy and safety of sonothombolysis versus non-sonothombolysis in patients with acute ischemic stroke: A meta-analysis of randomized controlled trials. PLoS One 2019;14(1) e0210516.
Childs RW, Carlsten M. Therapeutic approaches to enhance natural killer cell cytotoxicity against cancer: The force awakens. Nat Rev Drug Discov 2015;14:487–498.

Cho H, Lee HY, Han M, Choi JR, Ahn S, Lee T, Chang Y, Park J. Localized down-regulation of P-glycoprotein by focused ultrasound and microbubbles induced blood-brain barrier disruption in rat brain. Sci Rep 2016;6:31201.
Choi JJ, Carlisle RC, Coviello C, Seymour L, Coussios C-C. Non-invasive and real-time passive acoustic mapping of ultrasound-mediated drug delivery. Phys Med Biol 2014;59:4861–4877.
Cowley J, McGinty S. A mathematical model of sonoporation using a liquid-crystalline shelled microbubble. Ultrasonics 2019;96:214–219.
Crake C, Brinker ST, Coviello CM, Livingstone MS, McDannold NJ. A dual-mode hemispherical sparse array for 3D passive acoustic mapping and skull localization within a clinical MRI guided focused ultrasound device. Phys Med Biol 2018;63 065008.
Daecher A, Stanczak M, Liu JB, Zhang J, Du SS, Forsberg F, Leeper DB, Eisenbrey JR. Localized microbubble cavitation-based antivascular therapy for improving HCC treatment response to radiotherapy. Cancer Lett 2017;411:100–105.
Datta S, Coussios CC, McAdory LE, Tan J, Porter T, De Courten-Myers G, Holland CK. Correlation of cavitation with ultrasound enhancement of thrombolysis. Ultrasound Med Biol 2006;32:1257–1267.
Dayton P, Klibanov A, Brandenburger G, Ferrara K. Acoustic radiation force in vivo: A mechanism to assist targeting of microbubbles. Ultrasound Med Biol 1999;25:1195–1201.
De Cock I, Zagato E, Braeckmans K, Luan Y, de Jong N, De Smedt SC, Lentacker I. Ultrasound and microbubble mediated drug delivery: Acoustic pressure as determinant for uptake *via* membrane pores or endocytosis. J Control Release 2015;197:20–28.
De Saint Victor MD, Barnsley LC, Carugo D, Owen J, Coussios CC, Stride E. Sonothrombolysis with magnetically targeted microbubbles. Ultrasound Med Biol 2019;45:1151–1163.
Deffieux T, Montaldo G, Tanter M, Fink M. Shear wave spectroscopy for in vivo quantification of human soft tissues visco-elasticity. IEEE Trans Med Imaging 2009;28:313–322.
Definity. Silver Spring. MD: U.S. Food and Drug Administration; 2011.
Deng J, Huang Q, Wang F, Liu Y, Wang Z, Zhang Q, Lei B, Cheng Y. The role of caveolin-1 in blood-brain barrier disruption induced by focused ultrasound combined with microbubbles. J Mol Neurosci 2012;46:677–687.
Deng Q, Hu B, Cao S, Song HN, Chen JL, Zhou Q. Improving the efficacy of therapeutic angiogenesis by UTMD-mediated Ang-1 gene delivery to the infarcted myocardium. Int J Mol Med 2015;36:335–344.
Deng L, O'Reilly MA, Jones RM, An R, Hynynen K. A multi-frequency sparse hemispherical ultrasound phased array for microbubble-mediated transcranial therapy and simultaneous cavitation mapping. Phys Med Biol 2016;61:8476–8501.
Dewitte H, Van Lint S, Heirman C, Thielemans K, De Smedt SC, Breckpot K, Lentacker I. The potential of antigen and TriMix sonoporation using mRNA-loaded microbubbles for ultrasound-triggered cancer immunotherapy. J Control Release 2014;194:28–36.
Dewitte H, Vanderperren K, Haers H, Stock E, Duchateau L, Hesta M, Saunders JH, De Smedt SC, Lentacker I, De SC. Theranostic mRNA-loaded microbubbles in the lymphatics of dogs: Implications for drug delivery. Theranostics 2015;5:97–109.
Dimcevski G, Kotopoulis S, Bjanes T, Hoem D, Schjott J, Gjertsen BT, Biermann M, Molven A, Sorbye H, McCormack E, Postema M, Gilja OH. A human clinical trial using ultrasound and microbubbles to enhance gemcitabine treatment of inoperable pancreatic cancer. J Control Release 2016;243:172–181.
Dixon AJ, Li J, Rickel JMR, Klibanov AL, Zuo ZY, Hossack JA. Efficacy of sonothrombolysis using microbubbles produced by a catheter-based microfluidic device in a rat model of ischemic stroke. Ann Biomed Eng 2019;47:1012–1022.
Doinikov AA, Bouakaz A. Theoretical investigation of shear stress generated by a contrast microbubble on the cell membrane as a mechanism for sonoporation. J Acoust Soc Am 2010;128:11–19.
Dollet B, Marmottant P, Garbin V. Bubble dynamics in soft and biological matter. Annu Rev Fluid Mech 2019;51:331–355.
Dong Y, Xu Y, Li P, Wang C, Cao Y, Yu J. Antibiofilm effect of ultrasound combined with microbubbles against *Staphylococcus epidermidis* biofilm. Int J Med Microbiol 2017;307:321–328.
Dong Y, Li J, Li P, Yu J. Ultrasound microbubbles enhance the activity of vancomycin against *Staphylococcus epidermidis* biofilms in vivo. J Ultrasound Med 2018;37:1379–1387.
Downs ME, Buch A, Sierra C, Karakatsani ME, Teichert T, Chen S, Konofagou EE, Ferrera VP. Long-term safety of repeated blood-brain barrier opening via focused ultrasound with microbubbles in non-human primates performing a cognitive task. PLoS One 2015;10 e0125911.
Dumantepe M, Uyar I, Teymen B, Ugur O, Enc Y. Improvements in pulmonary artery pressure and right ventricular function after ultrasound-accelerated catheter-directed thrombolysis for the treatment of pulmonary embolism. J Cardiac Surg 2014;29:455–463.
Ebben HP, Nederhoed JH, Lely RJ, Wisselink W, Yeung K, Collaborators M. Microbubbles and ultrasound-accelerated thrombolysis (MUST) for peripheral arterial occlusions: Protocol for a phase II single-arm trial. BMJ Open 2017;7(8) e014365.
Eggen S, Fagerland SM, Mørch Ý, Hansen R, Søvik K, Berg S, Furu H, Bøhn AD, Lilledahl MB, Angelsen A, Angelsen B, de Lange Davies C. Ultrasound-enhanced drug delivery in prostate cancer xenografts by nanoparticles stabilizing microbubbles. J Control Release 2014;187:39–49.
Elder SA. Cavitation microstreaming. J Acoust Soc Am 1958;31:54–64.
Engelberger RP, Kucher N. Ultrasound-assisted thrombolysis for acute pulmonary embolism: A systematic review. Eur Heart J 2014;35:758–764.
Escoffre JM, Mannaris C, Geers B, Novell A, Lentacker I, Averkiou M, Bouakaz A. Doxorubicin liposome-loaded microbubbles for contrast imaging and ultrasound-triggered drug delivery. IEEE Trans Ultrason Ferroelectr Freq Control 2013;60:78–87.
Everbach EC, Francis CW. Cavitational mechanisms in ultrasound-accelerated thrombolysis at 1 MHz. Ultrasound Med Biol 2000;26:1153–1160.
Faez T, Emmer M, Kooiman K, Versluis M, van der Steen AF, de Jong N. 20 years of ultrasound contrast agent modeling. IEEE Trans Ultrason Ferroelectr Freq Control 2013;60:7–20.
Fan Z, Liu H, Mayer M, Deng CX. Spatiotemporally controlled single cell sonoporation. Proc Natl Acad Sci USA 2012;109:16486–16491.
Fan Z, Chen D, Deng CX. Improving ultrasound gene transfection efficiency by controlling ultrasound excitation of microbubbles. J Control Release 2013;170:401–413.
Fekri F, Delos Santos RC, Karshafian R, Antonescu CN. Ultrasound microbubble treatment enhances clathrin-mediated endocytosis and fluid-phase uptake through distinct mechanisms. PLoS One 2016;11 e0156754.
Ferrara KW, Borden MA, Zhang H. Lipid-shelled vehicles: Engineering for ultrasound molecular imaging and drug delivery. Acc Chem Res 2009;42:881–892.
Fix SM, Papadopoulou V, Velds H, Kasoji SK, Rivera JN, Borden MA, Chang S, Dayton PA. Oxygen microbubbles improve radiotherapy tumor control in a rat fibrosarcoma model - A preliminary study. PLoS One 2018;13(4) e0195667.
Fletcher SP, O'Reilly MA. Analysis of multifrequency and phase keying strategies for focusing ultrasound to the human vertebral canal. IEEE Trans Ultrason Ferroelectr Freq Control 2018;65:2322–2331.
Flight SM, Masci PP, Lavin MF, Gaffney PJ. Resistance of porcine blood clots to lysis relates to poor activation of porcine plasminogen by tissue plasminogen activator. Blood Coagul Fibrin 2006;17:417–420.
Flint EB, Suslick KS. The temperature of cavitation. Science 1991;253:1397–1399.
Flynn HG. Physics of acoustic cavitation in liquids. In: Mason WP, (ed). Physical acoustics. New York: Academic Press; 1964. p. 58–172.
Flynn HG. Cavitation dynamics: I. Mathematical formulation. J Acoust Soc Am 1975;57:1379–1396.
Flynn HG. Cavitation dynamics: II. Free pulsations and models for cavitation bubbles. J Acoust Soc Am 1975;58:1160–1170.
Flynn HG. Generation of transient cavities in liquids by microsecond pulses of ultrasound. J Acoust Soc Am 1982;72:1926–1932.
Forbes MM, O'Brien WD, Jr. Development of a theoretical model describing sonoporation activity of cells exposed to ultrasound in the presence of contrast agents. J Acoust Soc Am 2012;131:2723–2729.

Fu YY, Zhang L, Yang Y, Liu CW, He YN, Li P, Yu X. Synergistic antibacterial effect of ultrasound microbubbles combined with chitosan-modified polymyxin B-loaded liposomes on biofilm-producing *Acinetobacter baumannii*. Int J Nanomed 2019;14:1805–1815.
Gabriel DA, Muga K, Boothroyd EM. The effect of fibrin structure on fibrinolysis. J Biol Chem 1992;267:24259–24263.
Garcia MJ. Endovascular management of acute pulmonary embolism using the ultrasound-enhanced EkoSonic System. Semin Interv Radiol 2015;32:384–387.
Gauberti M. Reperfusion in acute ischaemic stroke by sonothrombolysis. Lancet Neurol 2019;18:320–321.
Goertz DE. An overview of the influence of therapeutic ultrasound exposures on the vasculature: High intensity ultrasound and microbubble-mediated bioeffects. Int J Hyperthermia 2015;31:134–144.
Goh BHT, Conneely M, Kneupner H, Palmer T, Klaseboer E, Khoo BC, Campbell P. High-speed imaging of ultrasound-mediated bacterial biofilm disruption. 6th European Conference of the International Federation for Medical and Biological Engineering. Cham: Springer International; 2015. p. 533–536.
Goutal S, Gerstenmayer M, Auvity S, Caillé F, Mériaux S, Buvat I, Larrat B, Tournier N. Physical blood-brain barrier disruption induced by focused ultrasound does not overcome the transporter-mediated efflux of erlotinib. J Control Release 2018;292:210–220.
Goyal A, Yu FTH, Tenwalde MG, Chen XC, Althouse A, Villanueva FS, Pacella JJ. Inertial cavitation ultrasound with microbubbles improves reperfusion efficacy when combined with tissue plasminogen activator in an in vitro model of microvascular obstruction. Ultrasound Med Biol 2017;43:1391–1400.
Graham SM, Carlisle R, Choi JJ, Stevenson M, Shah AR, Myers RS, Fisher K, Peregrino MB, Seymour L, Coussios CC. Inertial cavitation to non-invasively trigger and monitor intratumoral release of drug from intravenously delivered liposomes. J Control Release 2014;178:101–107.
Gras Navarro A, Bjorklund AT, Chekenya M. Therapeutic potential and challenges of natural killer cells in treatment of solid tumors. Front Immunol 2015;6:202.
Guo H, Wang Z, Du Q, Li P, Wang Z, Wang A. Stimulated phase-shift acoustic nanodroplets enhance vancomycin efficacy against methicillin-resistant *Staphylococcus aureus* biofilms. Int J Nanomed 2017;12:4679–4690.
Guo X, Cai C, Xu G, Yang Y, Tu J, Huang P, Zhang D. Interaction between cavitation microbubble and cell: A simulation of sonoporation using boundary element method (BEM). Ultrason Sonochem 2017;39:863–871.
Gupta R, Shea J, Scafe C, Shurlygina A, Rapoport N. Polymeric micelles and nanoemulsions as drug carriers: Therapeutic efficacy, toxicity, and drug resistance. J Control Release 2015;212:70–77.
Gyöngy M, Coussios CC. Passive cavitation mapping for localization and tracking of bubble dynamics. J Acoust Soc Am 2010;128: EL175–EL180.
Hamilton MF, Blackstock DT. Nonlinear acoustics. Melville, NY: Acoustical Society of America; 2008.
Han YW, Ikegami A, Chung P, Zhang L, Deng CX. Sonoporation is an efficient tool for intracellular fluorescent dextran delivery and one-step double-crossover mutant construction in *Fusobacterium nucleatum*. Appl Environ Microbiol 2007;73:3677–3683.
Haworth KJ, Bader KB, Rich KT, Holland CK, Mast TD. Quantitative frequency-domain passive cavitation imaging. IEEE Trans Ultrason Ferroelectr Freq Control 2017;64:177–191.
He Y, Zhang B, Chen Y, Jin Q, Wu J, Yan F, Zheng H. Image-guided hydrogen gas delivery for protection from myocardial ischemia−reperfusion injury via microbubbles. ACS Appl Mater Interfaces 2017;9:21190–21199.
Helfield B, Chen X, Watkins SC, Villanueva FS. Biophysical insight into mechanisms of sonoporation. Proc Natl Acad Sci USA 2016;113:9983–9988.
Hilgenfeldt S, Lohse D, Zomack M. Sound scattering and localized heat deposition of pulse-driven microbubbles. J Acoust Soc Am 2000;107:3530–3539.
Hitchcock KE, Ivancevich NM, Haworth KJ, Stamper DNC, Vela DC, Sutton JT, Pyne-Geithman GJ, Holland CK. Ultrasound-enhanced rt-PA thrombolysis in an ex vivo porcine carotid artery model. Ultrasound Med Biol 2011;37:1240–1251.
Ho YJ, Wang TC, Fan CH, Yeh CK. Spatially uniform tumor treatment and drug penetration by regulating ultrasound with microbubbles. ACS Appl Mater Interfaces 2018;10:17784–17791.
Holt RG, Roy RA. Measurements of bubble-enhanced heating from focused, MHz-frequency ultrasound in a tissue-mimicking material. Ultrasound Med Biol 2001;27:1399–1412.
Horsley H, Owen J, Browning R, Carugo D, Malone-Lee J, Stride E, Rohn JL. Ultrasound-activated microbubbles as a novel intracellular drug delivery system for urinary tract infection. J Control Release 2019;301:166–175.
Hosseinkhah N, Goertz DE, Hynynen K. Microbubbles and blood-brain barrier opening: A numerical study on acoustic emissions and wall stress predictions. IEEE Trans Biomed Eng 2015;62:1293–1304.
Hu X, Kheirolomoom A, Mahakian LM, Beegle JR, Kruse DE, Lam KS, Ferrara KW. Insonation of targeted microbubbles produces regions of reduced blood flow within tumor vasculature. Invest Radiol 2012;47:398–405.
Hu Y, Wan JM, Yu AC. Membrane perforation and recovery dynamics in microbubble-mediated sonoporation. Ultrasound Med Biol 2013;39:2393–2405.
Hu J, Zhang N, Jr, Li L, Zhang N, Sr, Ma Y, Zhao C, Wu Q, Li Y, He N, Wang X. The synergistic bactericidal effect of vancomycin on UTMD treated biofilm involves damage to bacterial cells and enhancement of metabolic activities. Sci Rep 2018;8:192.
Hu W, Wang G, Huang D, Sui M, Xu Y. Cancer immunotherapy based on natural killer cells: Current progress and new opportunities. Front Immunol 2019;10:1205.
Huang SW, Shekhar H, Holland CK. Comparative lytic efficacy of rt-PA and ultrasound in porcine versus human clots. PLoS One 2017;12(5) e0177786.
Hunt SJ, Gade T, Soulen MC, Pickup S, Sehgal CM. Antivascular ultrasound therapy: Magnetic resonance imaging validation and activation of the immune response in murine melanoma. J Ultrasound Med 2015;34:275–287.
Hynynen K, McDannold N, Vykhodtseva N, Jolesz FA. Noninvasive MR imaging-guided focal opening of the blood-brain barrier in rabbits. Radiology 2001;220:640–646.
Idbaih A, Canney M, Belin L, Desseaux C, Vignot A, Bouchoux G, Asquier N, Law-Ye B, Leclercq D, Bissery A, De Rycke Y, Trosch C, Capelle L, Sanson M, Hoang-Xuan K, Dehais C, Houillier C, Laigle-Donadey F, Mathon B, Andre A, Lafon C, Chapelon JY, Delattre JY, Carpentier A. Safety and feasibility of repeated and transient blood-brain barrier disruption by pulsed ultrasound in patients with recurrent glioblastoma. Clin Cancer Res 2019;25:3793–3801.
Jia C, Xu L, Han T, Cai P, Yu ACH, Qin P. Generation of reactive oxygen species in heterogeneously sonoporated cells by microbubbles with single-pulse ultrasound. Ultrasound Med Biol 2018;44:1074–1085.
Jones RM, O'Reilly MA, Hynynen K. Transcranial passive acoustic mapping with hemispherical sparse arrays using CT-based skull-specific aberration corrections: A simulation study. Phys Med Biol 2013;58:4981–5005.
Jones RM, O'Reilly MA, Hynynen K. Experimental demonstration of passive acoustic imaging in the human skull cavity using CT-based aberration corrections. Med Phys 2015;42:4385–4400.
Jones RM, Deng L, Leung K, McMahon D, O'Reilly MA, Hynynen K. Three-dimensional transcranial microbubble imaging for guiding volumetric ultrasound-mediated blood-brain barrier opening. Theranostics 2018;8:2909–2926.
Jordão JF, Thévenot E, Markham-Coultes K, Scarcelli T, Weng YQ, Xhima K, O'Reilly M, Huang Y, McLaurin J, Hynynen K, Aubert I. Amyloid-β plaque reduction, endogenous antibody delivery and glial activation by brain-targeted, transcranial focused ultrasound. Exp Neurol 2013;248:16–29.
Juang EK, De Cock I, Keravnou C, Gallagher MK, Keller SB, Zheng Y, Averkiou M. Engineered 3D microvascular networks for the study of ultrasound-microbubble-mediated drug delivery. Langmuir 2019;35:10128–10138.
Junttila MR, de Sauvage FJ. Influence of tumour micro-environment heterogeneity on therapeutic response. Nature 2013;501:346–354.

Kamimura HA, Flament J, Valette J, Cafarelli A, Aron Badin R, Hantraye P, Larrat B. Feedback control of microbubble cavitation for ultrasound-mediated blood-brain barrier disruption in non-human primates under magnetic resonance guidance. J Cereb Blood Flow Metab 2019;39:1191–1203.

Keravnou CP, De Cock I, Lentacker I, Izamis ML, Averkiou MA. Microvascular injury and perfusion changes induced by ultrasound and microbubbles in a machine-perfused pig liver. Ultrasound Med Biol 2016;42:2676–2686.

Khalil DN, Smith EL, Brentjens RJ, Wolchok JD. The future of cancer treatment: Immunomodulation, CARs and combination immunotherapy. Nat Rev Clin Oncol 2016;13:394.

Kilroy JP, Klibanov AL, Wamhoff BR, Bowles DK, Hossack JA. Localized in vivo model drug delivery with intravascular ultrasound and microbubbles. Ultrasound Med Biol 2014;40:2458–2467.

Kilroy JP, Dhanaliwala AH, Klibanov AL, Bowles DK, Wamhoff BR, Hossack JA. Reducing neointima formation in a swine model with IVUS and sirolimus microbubbles. Ann Biomed Eng 2015;43:2642–2651.

Kim H, Britton GL, Peng T, Holland CK, McPherson DD, Huang SL. Nitric oxide-loaded echogenic liposomes for treatment of vasospasm following subarachnoid hemorrhage. Int J Nanomed 2014;9:155–165.

Kleven RT, Karani KB, Salido NG, Shekhar H, Haworth KJ, Mast TD, Tadesse DG, Holland CK. The effect of 220 kHz insonation scheme on rt-PA thrombolytic efficacy in vitro. Phys Med Biol 2019;64 165015.

Kolb J, Nyborg WL. Small-scale acoustic streaming in liquids. J Acoust Soc Am 1956;28:1237–1242.

Kooiman K, Vos HJ, Versluis M, de Jong N. Acoustic behavior of microbubbles and implications for drug delivery. Adv Drug Deliv Rev 2014;72C:28–48.

Kopechek JA, Park E, Mei CS, McDannold NJ, Porter TM. Accumulation of phase-shift nanoemulsions to enhance MR-guided ultrasound-mediated tumor ablation in vivo. J Healthc Eng 2013;4:109–126.

Kopechek JA, Park EJ, Zhang YZ, Vykhodtseva NI, McDannold NJ, Porter TM. Cavitation-enhanced MR-guided focused ultrasound ablation of rabbit tumors in vivo using phase shift nanoemulsions. Phys Med Biol 2014;59:3465–3481.

Kopechek JA, Carson AR, McTiernan CF, Chen X, Hasjim B, Lavery L, Sen M, Grandis JR, Villanueva FS. Ultrasound targeted microbubble destruction-mediated delivery of a transcription factor decoy inhibits STAT3 signaling and tumor growth. Theranostics 2015;5:1378–1387.

Koshiyama K, Wada S. Molecular dynamics simulations of pore formation dynamics during the rupture process of a phospholipid bilayer caused by high-speed equibiaxial stretching. J Biomech 2011;44:2053–2058.

Kotopoulis S, Dimcevski G, Gilja OH, Hoem D, Postema M. Treatment of human pancreatic cancer using combined ultrasound, microbubbles, and gemcitabine: A clinical case study. Med Phys 2013;40 072902.

Kotopoulis S, Stigen E, Popa M, Safont MM, Healey A, Kvåle S, Sontum P, Gjertsen BT, Gilja OH, McCormack E. Sonoporation with Acoustic Cluster Therapy (ACT) induces transient tumour volume reduction in a subcutaneous xenograft model of pancreatic ductal adenocarcinoma. J Control Release 2017;245:70–80.

Kovacs ZI, Burks SR, Frank JA. Reply to Silburt et al.: Concerning sterile inflammation following focused ultrasound and microbubbles in the brain. Proc Natl Acad Sci USA 2017;114:E6737–E6738.

Kovacs ZI, Kim S, Jikaria N, Qureshi F, Milo B, Lewis BK, Bresler M, Burks SR, Frank JA. Disrupting the blood-brain barrier by focused ultrasound induces sterile inflammation. Proc Natl Acad Sci USA 2017;114:E75–E84.

Kripfgans OD, Fowlkes JB, Miller DL, Eldevik OP, Carson PL. Acoustic droplet vaporization for therapeutic and diagnostic applications. Ultrasound Med Biol 2000;26:1177–1189.

Kudo N. High-Speed In Situ Observation System for Sonoporation of Cells With Size- and Position-Controlled Microbubbles. IEEE Trans Ultrason Ferroelectr Freq Control 2017;64:273–280.

Kudo N, Kinoshita Y. Effects of cell culture scaffold stiffness on cell membrane damage induced by sonoporation. J Med Ultrason 2014;41:411–420.

Lai P, Tarapacki C, Tran WT, El Kaffas A, Lee J, Hupple C, Iradji S, Giles A, Al-Mahrouki A, Czarnota GJ. Breast tumor response to ultrasound mediated excitation of microbubbles and radiation therapy in vivo. Oncoscience 2016;3:98–108.

Lammers T, Kiessling F, Hennink WE, Storm G. Drug targeting to tumors: Principles, pitfalls and (pre-) clinical progress. J Control Release 2012;161:175–187.

Lattwein KR, Shekhar H, van Wamel WJB, Gonzalez T, Herr AB, Holland CK, Kooiman K. An in vitro proof-of-principle study of sonobactericide. Sci Rep 2018;8:3411.

Lattwein KR, Shekhar H, Kouijzer JJP, van Wamel WJB, Holland CK, Kooiman K. Sonobactericide: An emerging treatment strategy for bacterial infections. Ultrasound Med Biol 2020;46:193–215.

Lea-Banks H, Teo B, Stride E, Coussios CC. The effect of particle density on ultrasound-mediated transport of nanoparticles. Phys Med Biol 2016;61:7906–7918.

Lea-Banks H, O'Reilly MA, Hynynen K. Ultrasound-responsive droplets for therapy: A review. J Control Release 2019;293:144–154.

Lee PJ, Rudenko D, Kuliszewski MA, Liao C, Kabir MG, Connelly KA, Leong-Poi H. Surviving gene therapy attenuates left ventricular systolic dysfunction in doxorubicin cardiomyopathy by reducing apoptosis and fibrosis. Cardiovasc Res 2014;101:423–433.

Lee KA, Cha A, Kumar MH, Rezayat C, Sales CM. Catheter-directed, ultrasound-assisted thrombolysis is a safe and effective treatment for pulmonary embolism, even in high-risk patients. J Vasc Surg Venous Lymphat Disord 2017;5:165–170.

Leinenga G, Götz J. Scanning ultrasound removes amyloid-β and restores memory in an Alzheimer's disease mouse model. Sci Transl Med 2015;7 278.ra33.

Lentacker I, De Smedt SC, Sanders NN. Drug loaded microbubble design for ultrasound triggered delivery. Soft Matter 2009;5:2161–2170.

Lentacker I, De Cock I, Deckers R, De Smedt SC, Moonen CT. Understanding ultrasound induced sonoporation: Definitions and underlying mechanisms. Adv Drug Deliv Rev 2014;72:49–64.

Leow RS, Wan JM, Yu AC. Membrane blebbing as a recovery manoeuvre in site-specific sonoporation mediated by targeted microbubbles. J R Soc Interface 2015;12 pii: 20150029.

Li W, Yuan T, Xia-Sheng G, Di X, Dong Z. Microstreaming velocity field and shear stress created by an oscillating encapsulated microbubble near a cell membrane. Chin Phys B 2014;23 124302.

Li S, Zhu C, Fang S, Zhang W, He N, Xu W, Kong R, Shang X. Ultrasound microbubbles enhance human beta-defensin 3 against biofilms. J Surg Res 2015;199:458–469.

Liao AH, Hung CR, Lin CF, Lin YC, Chen HK. Treatment effects of lysozyme-shelled microbubbles and ultrasound in inflammatory skin disease. Sci Rep 2017;7:41325.

Lin T, Cai XZ, Shi MM, Ying ZM, Hu B, Zhou CH, Wang W, Shi ZL, Yan SG. In vitro and in vivo evaluation of vancomycin-loaded PMMA cement in combination with ultrasound and microbubbles-mediated ultrasound. Biomed Res Int 2015;2015 309739.

Lipsman N, Meng Y, Bethune AJ, Huang Y, Lam B, Masellis M, Herrmann N, Heyn C, Aubert I, Boutet A, Smith GS, Hynynen K, Black SE. Blood-brain barrier opening in Alzheimer's disease using MR-guided focused ultrasound. Nat Commun 2018;9:2336.

Liu HL, Hsieh HY, Lu LA, Kang CW, Wu MF, Lin CY. Low-pressure pulsed focused ultrasound with microbubbles promotes an anticancer immunological response. J Transl Med 2012;10:221.

Liu Y, Li L, Su Q, Liu T, Ma Z, Yang H. Ultrasound-targeted microbubble destruction enhances gene expression of microRNA-21 in swine heart via intracoronary delivery. Echocardiography 2015;32:1407–1416.

Liu HL, Jan CK, Tsai CH, Huang SM, Li ML, Qui W, Zheng H. Design and implementation of a dual-transmit/receive-mode therapeutic ultrasound phased array system for brain therapy. Proc IEEE Ultrason Symp 2018; Available at: https://ieeexplore.ieee.org/document/8579682.

Liu JX, Xu FF, Huang J, Xu JS, Liu Y, Yao YZ, Ao M, Li A, Hao L, Cao Y, Hu ZQ, Ran HT, Wang ZG, Li P. Low-intensity focused

ultrasound (LIFU)-activated nanodroplets as a theranostic agent for noninvasive cancer molecular imaging and drug delivery. Biomater Sci 2018;6:2838–2849.
Long DM, Multer FK, Greenburg AG, Peskin GW, Lasser EC, Wickham WG, Sharts CM. Tumor imaging with x-rays using macrophage uptake of radiopaque fluorocarbon emulsions. Surgery 1978;84:104–112.
Lumason. Silver Spring. MD: U.S. Food and Drug Administration; 2016.
Luo WX, Wen G, Yang L, Tang J, Wang JG, Wang JH, Zhang SY, Zhang L, Ma F, Xiao LL, Wang Y, Li YJ. Dual-targeted and pH-sensitive doxorubicin prodrug-microbubble complex with ultrasound for tumor treatment. Theranostics 2017;7:452–465.
Madanshetty SI, Roy RA, Apfel RE. Acoustic Microcavitation—Its active and passive acoustic detection. J Acoust Soc Am 1991;90: 1515–1526.
Maeda H. Macromolecular therapeutics in cancer treatment: The EPR effect and beyond. J Control Release 2012;164:138–144.
Mainprize T, Lipsman N, Huang Y, Meng Y, Bethune A, Ironside S, Heyn C, Alkins R, Trudeau M, Sahgal A, Perry J, Hynynen K. Blood–brain barrier opening in primary brain tumors with non-invasive MR-guided focused ultrasound: A clinical safety and feasibility study. Sci Rep 2019;9:321.
Man VH, Truong PM, Li MS, Wang J, Van-Oanh NT, Derreumaux P, Nguyen PH. Molecular mechanism of the cell membrane pore formation induced by bubble stable cavitation. J Phys Chem B 2019;123:71–78.
Marmottant P, Hilgenfeldt S. Controlled vesicle deformation and lysis by single oscillating bubbles. Nature 2003;423:153–156.
Marty B, Larrat B, Van Landeghem M, Robic C, Robert P, Port M, Le Bihan D, Pernot M, Tanter M, Lethimonnier F, Meriaux S. Dynamic study of blood-brain barrier closure after its disruption using ultrasound: A quantitative analysis. J Cereb Blood Flow Metab 2012;32:1948–1958.
Mathias W, Tsutsui JM, Tavares BG, Xie F, Aguiar MOD, Garcia DR, Oliveira MT, Soeiro A, Nicolau JC, Neto PAL, Rochitte CE, Ramires JAF, Kalil R, Porter TR. Diagnostic ultrasound impulses improve microvascular flow in patients with STEMI receiving intravenous microbubbles. J Am Coll Cardiol 2016;67:2506–2515.
Mathias W, Tsutsui JM, Tavares BG, Fava AM, Aguiar MOD, Borges BC, Oliveira MT, Soeiro A, Nicolau JC, Ribeiro HB, Chiang HP, Sbano JCN, Morad A, Goldsweig A, Rochitte CE, Lopes BBC, Ramirez JAF, Kalil R, Porter TR, Investigators M. Sonothrombolysis in ST-segment elevation myocardial infarction treated with primary percutaneous coronary intervention. J Am Coll Cardiol 2019;73:2832–2842.
Maxwell AD, Cain CA, Duryea AP, Yuan LQ, Gurm HS, Xu Z. Noninvasive thrombolysis using pulsed ultrasound cavitation therapy—Histotripsy. Ultrasound Med Biol 2009;35:1982–1994.
McDannold N, Vykhodtseva N, Hynynen K. Targeted disruption of the blood–brain barrier with focused ultrasound: Association with cavitation activity. Phys Med Biol 2006;51:793–807.
McDannold N, Arvanitis CD, Vykhodtseva N, Livingstone MS. Temporary disruption of the blood-brain barrier by use of ultrasound and microbubbles: Safety and efficacy evaluation in rhesus macaques. Cancer Res 2012;72:3652–3663.
McEwan C, Owen J, Stride E, Fowley C, Nesbitt H, Cochrane D, Coussios CC, Borden M, Nomikou N, McHale AP, Callan JF. Oxygen carrying microbubbles for enhanced sonodynamic therapy of hypoxic tumours. J Control Release 2015;203:51–56.
McEwan C, Kamila S, Owen J, Nesbitt H, Callan B, Borden M, Nomikou N, Hamoudi RA, Taylor MA, Stride E, McHale AP, Callan JF. Combined sonodynamic and antimetabolite therapy for the improved treatment of pancreatic cancer using oxygen loaded microbubbles as a delivery vehicle. Biomaterials 2016;80:20–32.
McMahon D, Hynynen K. Acute inflammatory response following increased blood-brain barrier permeability induced by focused ultrasound is dependent on microbubble dose. Theranostics 2017;7:3989–4000.
McMahon D, Mah E, Hynynen K. Angiogenic response of rat hippocampal vasculature to focused ultrasound-mediated increases in blood-brain barrier permeability. Sci Rep 2018;8:12178.
Mead BP, Mastorakos P, Suk JS, Klibanov AL, Hanes J, Price RJ. Targeted gene transfer to the brain via the delivery of brain-penetrating DNA nanoparticles with focused ultrasound. J Control Release 2016;223:109–117.
Mead BP, Kim N, Miller GW, Hodges D, Mastorakos P, Klibanov AL, Mandell JW, Hirsh J, Suk JS, Hanes J, Price RJ. Novel focused ultrasound gene therapy approach noninvasively restores dopaminergic neuron function in a rat Parkinson's disease model. Nano Lett 2017;17:3533–3542.
Mehta G, Hsiao AY, Ingram M, Luker GD, Takayama S. Opportunities and challenges for use of tumor spheroids as models to test drug delivery and efficacy. J Control Release 2012;164:192–204.
Min HS, Son S, You DG, Lee TW, Lee J, Lee S, Yhee JY, Lee J, Han MH, Park JH, Kim SH, Choi K, Park K, Kim K, Kwon IC. Chemical gas-generating nanoparticles for tumor-targeted ultrasound imaging and ultrasound-triggered drug delivery. Biomaterials 2016;108:57–70.
Molina CA, Ribo M, Rubiera M, Montaner J, Santamarina E, Delgado-Mederos R, Arenillas JF, Huertas R, Purroy F, Delgado P, Alvarez-Sabin J. Microbubble administration accelerates clot lysis during continuous 2-MHz ultrasound monitoring in stroke patients treated with intravenous tissue plasminogen activator. Stroke 2006;37:425–429.
Monteith S, Sheehan J, Medel R, Wintermark M, Eames M, Snell J, Kassell NF, Elias WJ. Potential intracranial applications of magnetic resonance-guided focused ultrasound surgery. J Neurosurg 2013;118:215–221.
Montero AS, Bielle F, Goldwirt L, Lalot A, Bouchoux G, Canney M, Belin F, Beccaria K, Pradat PF, Salachas F, Boillée S, Lobsiger C, Lafon C, Chapelon JY, Carpentier A. Ultrasound-induced blood-spinal cord barrier opening in rabbits. Ultrasound Med Biol 2019;45:2417–2426.
Mooney SJ, Shah K, Yeung S, Burgess A, Aubert I, Hynynen K. Focused Ultrasound-Induced Neurogenesis Requires an Increase in Blood-Brain Barrier Permeability. PLoS One 2016;11 e0159892.
Myers R, Coviello C, Erbs P, Foloppe J, Rowe C, Kwan J, Crake C, Finn S, Jackson E, Balloul JM, Story C, Coussios C, Carlisle R. Polymeric cups for cavitation-mediated delivery of oncolytic vaccinia virus. Mol Ther 2016;24:1627–1633.
Naudé CF, Ellis AT. On the mechanism of cavitation damage by non-hemispherical cavities collapsing in contact with a solid boundary. J Basic Eng 1961;83:648–656.
Nesbitt H, Sheng Y, Kamila S, Logan K, Thomas K, Callan B, Taylor MA, Love M, O'Rourke D, Kelly P, Beguin E, Stride E, McHale AP, Callan JF. Gemcitabine loaded microbubbles for targeted chemo-sonodynamic therapy of pancreatic cancer. J Control Release 2018;279:8–16.
Nolsøe CP, Lorentzen T. International guidelines for contrast-enhanced ultrasonography: Ultrasound imaging in the new millennium. Ultrasonography 2016;35:89–103.
Nowbar AN, Gitto M, Howard JP, Francis DP, Al-Lamee R. Mortality From ischemic heart disease: Analysis of data from the World Health Organization and coronary artery disease risk factors from NCD risk factor collaboration. Circ Cardiovasc Qual Outcomes 2019;12(6) e005375.
Nyborg WL. Acoustic streaming near a boundary. J Acoust Soc Am 1958;30:329–339.
O'Reilly MA, Hynynen K. Blood–brain barrier: Real-time feedback-controlled focused ultrasound disruption by using an acoustic emissions-based controller. Radiology 2012;263:96–106.
O'Reilly MA, Jones RM, Hynynen K. Three-dimensional transcranial ultrasound imaging of microbubble clouds using a sparse hemispherical array. IEEE Trans Biomed Eng 2014;61:1285–1294.
O'Reilly MA, Chinnery T, Yee ML, Wu SK, Hynynen K, Kerbel RS, Czarnota GJ, Pritchard KI, Sahgal A. Preliminary investigation of focused ultrasound-facilitated drug delivery for the treatment of leptomeningeal metastases. Sci Rep 2018;8:9013.
Optison. Silver Spring. MD: U.S. Food and Drug Administration; 2012.
Paefgen V, Doleschel D, Kiessling F. Evolution of contrast agents for ultrasound imaging and ultrasound-mediated drug delivery. Front Pharmacol 2015;6:197.
Pandit R, Leinenga G, Götz J. Repeated ultrasound treatment of tau transgenic mice clears neuronal tau by autophagy and improves behavioral functions. Theranostics 2019;9:3754–3767.

Pardridge WM. The blood-brain barrier: Bottleneck in brain drug development. NeuroRx 2005;2:3–14.
Paris JL, Mannaris C, Cabanas MV, Carlisle R, Manzano M, Vallet-Regi M, Coussios CC. Ultrasound-mediated cavitation-enhanced extravasation of mesoporous silica nanoparticles for controlled-release drug delivery. Chem Eng J 2018;340:2–8.
Park EJ, Zhang YZ, Vykhodtseva N, McDannold N. Ultrasound-mediated blood-brain/blood-tumor barrier disruption improves outcomes with trastuzumab in a breast cancer brain metastasis model. J Control Release 2012;163:277–284.
Park YC, Zhang C, Kim S, Mohamedi G, Beigie C, Nagy JO, Holt RG, Cleveland RO, Jeon NL, Wong JY. Microvessels-on-a-chip to assess targeted ultrasound-assisted drug delivery. ACS Appl Mater Interfaces 2016;8:31541–31549.
Payne AH, Hawryluk GW, Anzai Y, Odéen H, Ostlie MA, Reichert EC, Stump AJ, Minoshima S, Cross DJ. Magnetic resonance imaging-guided focused ultrasound to increase localized blood-spinal cord barrier permeability. Neural Regen Res 2017;12:2045–2049.
Pereno V, Characterisation of microbubble-membrane interactions in ultrasound mediated drug delivery. D.Phil. Thesis, University of Oxford; 2018. https://ora.ox.ac.uk/objects/uuid:515f2c15-e9d3-46b8-875c-420084fbc9a3
Petit B, Bohren Y, Gaud E, Bussat P, Arditi M, Yan F, Tranquart F, Allemann E. Sonothrombolysis: The contribution of stable and inertial cavitation to clot lysis. Ultrasound Med Biol 2015;41:1402–1410.
Phelps AD, Leighton TG. The subharmonic oscillations and combination-frequency subharmonic emissions from a resonant bubble: Their properties and generation mechanisms. Acustica 1997;83:59–66.
Poon CT, Shah K, Lin C, Tse R, Kim KK, Mooney S, Aubert I, Stefanovic B, Hynynen K. Time course of focused ultrasound effects on β-amyloid plaque pathology in the TgCRND8 mouse model of Alzheimer's disease. Sci Rep 2018;8:14061.
Pouliopoulos AN, Choi JJ. Superharmonic microbubble Doppler effect in ultrasound therapy. Phys Med Biol 2016;61:6154–6171.
Prokop AF, Soltani A, Roy RA. Cavitational mechanisms in ultrasound-accelerated fibrinolysis. Ultrasound Med Biol 2007;33:924–933.
Prosperetti A. Thermal effects and damping mechanisms in forced radial oscillations of gas-bubbles in liquids. J Acoust Soc Am 1977;61:17–27.
Qian L, Thapa B, Hong J, Zhang Y, Zhu M, Chu M, Yao J, Xu D. The present and future role of ultrasound targeted microbubble destruction in preclinical studies of cardiac gene therapy. J Thorac Dis 2018;10:1099–1111.
Qin D, Zhang L, Chang N, Ni P, Zong Y, Bouakaz A, Wan M, Feng Y. In situ observation of single cell response to acoustic droplet vaporization: Membrane deformation, permeabilization, and blebbing. Ultrason Sonochem 2018;47:141–150.
Qin P, Han T, Yu ACH, Xu L. Mechanistic understanding the bioeffects of ultrasound-driven microbubbles to enhance macromolecule delivery. J Control Release 2018;272:169–181.
Radhakrishnan K, Holland CK, Haworth KJ. Scavenging dissolved oxygen via acoustic droplet vaporization. Ultrason Sonochem 2016;31:394–403.
Rapoport NY, Kennedy AM, Shea JE, Scaife CL, Nam KH. Controlled and targeted tumor chemotherapy by ultrasound-activated nanoemulsions/microbubbles. J Control Release 2009;138:268–276.
Ronan E, Edjiu N, Kroukamp O, Wolfaardt G, Karshafian R. USMB-induced synergistic enhancement of aminoglycoside antibiotics in biofilms. Ultrasonics 2016;69:182–190.
Roovers S, Lajoinie G, De Cock I, Brans T, Dewitte H, Braeckmans K, Versuis M, De Smedt SC, Lentacker I. Sonoprinting of nanoparticle-loaded microbubbles: Unraveling the multi-timescale mechanism. Biomaterials 2019;217 119250.
Roovers S, Lajoinie G, Prakash J, Versluis M, De Smedt SC, Lentacker I. Liposome-loaded microbubbles and ultrasound enhance drug delivery in a 3D tumor spheroid. Abstract book, 24th European Symposium on Ultrasound Contrast Imaging. Rotterdam: Erasmus MC; 2019. p. 27–31.
Roovers S, Segers T, Lajoinie G, Deprez J, Versluis M, De Smedt SC, Lentacker I. The role of ultrasound-driven microbubble dynamics in drug delivery: From microbubble fundamentals to clinical translation. Langmuir 2019;35:10173–10191.
Rosenthal I, Sostaric JZ, Riesz P. Sonodynamic therapy—A review of the synergistic effects of drugs and ultrasound. Ultrason Sonochem 2004;11:349–363.
Rossi S, Szíjjártó C, Gerber F, Waton G, Krafft MP. Fluorous materials in microbubble engineering science and technology—Design and development of new bubble preparation and sizing technologies. J Fluorine Chem 2011;132:1102–1109.
Rowlatt CF, Lind SJ. Bubble collapse near a fluid-fluid interface using the spectral element marker particle method with applications in bioengineering. Int J Multiphas Flow 2017;90:118–143.
Roy RA, Madanshetty SI, Apfel RE. An acoustic backscattering technique for the detection of transient cavitation produced by microsecond pulses of ultrasound. J Acoust Soc Am 1990;87:2451–2458.
Salgaonkar VA, Datta S, Holland CK, Mast TD. Passive cavitation imaging with ultrasound arrays. J Acoust Soc Am 2009;126:3071–3083.
Santos PM, Butterfield LH. Dendritic cell-based cancer vaccines. J Immunol 2018;200:443–449.
Scarcelli T, Jordão JF, O'Reilly MA, Ellens N, Hynynen K, Aubert I. Stimulation of hippocampal neurogenesis by transcranial focused ultrasound and microbubbles in adult mice. Brain Stimul 2014;7:304–307.
Schissler AJ, Gylnn RJ, Sobieszczyk PS, Waxman AB. Ultrasound-assisted catheter-directed thrombolysis compared with anticoagulation alone for treatment of intermediate-risk pulmonary embolism. Pulm Circ 2018;8(4) 2045894018800265.
Schneider M, Anantharam B, Arditi M, Bokor D, Broillet A, Bussat P, Fouillet X, Frinking P, Tardy I, Terrettaz J, Senior R, Tranquart F. BR38, a new ultrasound blood pool agent. Invest Radiol 2011;46:486–494.
Sever AR, Mills P, Jones SE, Mali W, Jones PA. Sentinel node identification using microbubbles and contrast-enhanced ultrasonography. Clin Radiol 2012;67:687–694.
Sever AR, Mills P, Weeks J, Jones SE, Fish D, Jones PA, Mali W. Preoperative needle biopsy of sentinel lymph nodes using intradermal microbubbles and contrast-enhanced ultrasound in patients with breast cancer. AJR Am J Roentgenol 2012;199:465–470.
Shamout FE, Pouliopoulos AN, Lee P, Bonaccorsi S, Towhidi L, Krams R, Choi JJ. Enhancement of non-invasive trans-membrane drug delivery using ultrasound and microbubbles during physiologically relevant flow. Ultrasound Med Biol 2015;41:2435–2448.
Sheeran PS, Dayton PA. Phase-change contrast agents for imaging and therapy. Curr Pharm Des 2012;18:2152–2165.
Sheikov N, McDannold N, Vykhodtseva N, Jolesz F, Hynynen K. Cellular mechanisms of the blood-brain barrier opening induced by ultrasound in presence of microbubbles. Ultrasound Med Biol 2004;30:979–989.
Sheikov N, McDannold N, Jolesz F, Zhang YZ, Tam K, Hynynen K. Brain arterioles show more active vesicular transport of blood-borne tracer molecules than capillaries and venules after focused ultrasound-evoked opening of the blood-brain barrier. Ultrasound Med Biol 2006;32:1399–1409.
Sheikov N, McDannold N, Sharma S, Hynynen K. Effect of focused ultrasound applied with an ultrasound contrast agent on the tight junctional integrity of the brain microvascular endothelium. Ultrasound Med Biol 2008;34:1093–1104.
Shekhar H, Bader KB, Huang SW, Peng T, Huang SL, McPherson DD, Holland CK. In vitro thrombolytic efficacy of echogenic liposomes loaded with tissue plasminogen activator and octafluoropropane gas. Phys Med Biol 2017;62:517–538.
Shekhar H, Kleven RT, Peng T, Palaniappan A, Karani KB, Huang SL, McPherson DD, Holland CK. In vitro characterization of sonothrombolysis and echocontrast agents to treat ischemic stroke. Sci Rep 2019;9:9902.
Shentu WH, Yan CX, Liu CM, Qi RX, Wang Y, Huang ZX, Zhou LM, You XD. Use of cationic microbubbles targeted to P-selectin to improve ultrasound-mediated gene transfection of hVEGF165 to the ischemic myocardium. J Zhejiang Univ Sci B 2018;19:699–707.
Shi YD, Shi WY, Chen L, Gu JP. A systematic review of ultrasound-accelerated catheter-directed thrombolysis in the treatment of deep vein thrombosis. J Thromb Thrombolysis 2018;45:440–451.

Shpak O, Verweij M, Vos HJ, de Jong N, Lohse D, Versluis M. Acoustic droplet vaporization is initiated by superharmonic focusing. Proc Natl Acad Sci USA 2014;111:1697–1702.
Shpak O, Verweij M, de Jong N, Versluis M. Droplets, bubbles and ultrasound interactions. Adv Exp Med Biol 2016;880:157–174.
Silburt J, Lipsman N, Aubert I. Disrupting the blood−brain barrier with focused ultrasound: Perspectives on inflammation and regeneration. Proc Natl Acad Sci USA 2017;114:E6735–E6736.
Silvestrini MT, Ingham ES, Mahakian LM, Kheirolomoom A, Liu Y, Fite BZ, Tam SM, Tucci ST, Watson KD, Wong AW, Monjazeb AM, Hubbard NE, Murphy WJ, Borowsky AD, Ferrara KW. Priming is key to effective incorporation of image-guided thermal ablation into immunotherapy protocols. JCI insight 2017;2:e90521.
Slikkerveer J, Juffermans LJM, van Royen N, Appelman Y, Porter TR, Kamp O. Therapeutic application of contrast ultrasound in ST elevation myocardial infarction: Role in coronary thrombosis and microvascular obstruction. Eur Heart J Acute Cardiovasc Care 2019;8:45–53.
Snipstad S, Berg S, Morch Y, Bjorkoy A, Sulheim E, Hansen R, Grimstad I, van Wamel A, Maaland AF, Torp SH, de Lange Davies C. Ultrasound improves the delivery and therapeutic effect of nanoparticle-stabilized microbubbles in breast cancer xenografts. Ultrasound Med Biol 2017;43:2651–2669.
Sontum P, Kvale S, Healey AJ, Skurtveit R, Watanabe R, Matsumura M, Ostensen J. Acoustic Cluster Therapy (ACT)—A novel concept for ultrasound mediated, targeted drug delivery. Int J Pharm 2015;495:1019–1027.
Sta Maria NS, Barnes SR, Weist MR, Colcher D, Raubitschek AA, Jacobs RE. Low dose focused ultrasound induces enhanced tumor accumulation of natural killer cells. PLoS One 2015;10 e0142767.
Steinman RM, Kaplan G, Witmer MD, Cohn ZA. Identification of a novel cell type in peripheral lymphoid organs of mice: V. Purification of spleen dendritic cells, new surface markers, and maintenance in vitro. J Exp Med 1979;149:1–16.
Stride E, Lajoinie G, Borden M, Versluis M, Cherkaoui S, Bettinger T, Segers T. Microbubble agents: New directions. Ultrasound in Medicine and Biology 2020; in press.
Su Q, Li L, Liu Y, Zhou Y, Wang J, Wen W. Ultrasound-targeted microbubble destruction-mediated microRNA-21 transfection regulated PDCD4/NF-kappaB/TNF-alpha pathway to prevent coronary microembolization-induced cardiac dysfunction. Gene Ther 2015;22:1000–1006.
Sugiyama MG, Mintsopoulos V, Raheel H, Goldenberg NM, Batt JE, Brochard L, Kuebler WM, Leong-Poi H, Karshafian R, Lee WL. Lung ultrasound and microbubbles enhance aminoglycoside efficacy and delivery to the lung in *Escherichia coli*-induced pneumonia and acute respiratory distress syndrome. Am J Respir Crit Care Med 2018;198:404–408.
Sun T, Zhang Y, Power C, Alexander PM, Sutton JT, Aryal M, Vykhodtseva N, Miller EL, McDannold NJ. Closed-loop control of targeted ultras;.pound drug delivery across the blood-brain/tumor barriers in a rat glioma model. Proc Natl Acad Sci USA 2017;114:E10281–E10290.
Sutton JT, Haworth KJ, Pyne-Geithman G, Holland CK. Ultrasound-mediated drug delivery for cardiovascular disease. Expert Opin Drug Deliv 2013;10:573–592.
Sutton JT, Raymond JL, Verleye MC, Pyne-Geithman GJ, Holland CK. Pulsed ultrasound enhances the delivery of nitric oxide from bubble liposomes to ex vivo porcine carotid tissue. Int J Nanomed 2014;9:4671–4683.
Tachibana K, Tachibana S. Albumin microbubble echo-contrast material as an enhancer for ultrasound accelerated thrombolysis. Circulation 1995;92:1148–1150.
Theek B, Baues M, Ojha T, Mockel D, Veettil SK, Steitz J, van Bloois L, Storm G, Kiessling F, Lammers T. Sonoporation enhances liposome accumulation and penetration in tumors with low EPR. J Control Release 2016;231:77–85.
Thevenot E, Jordao JF, O'Reilly MA, Markham K, Weng YQ, Foust KD, Kaspar BK, Hynynen K, Aubert I. Targeted delivery of self-complementary adeno-associated virus serotype 9 to the brain, using magnetic resonance imaging-guided focused ultrasound. Hum Gene Ther 2012;23:1144–1155.
Tian XQ, Ni XW, Xu HL, Zheng L, ZhuGe DL, Chen B, Lu CT, Yuan JJ, Zhao YZ. Prevention of doxorubicin-induced cardiomyopathy using targeted MaFGF mediated by nanoparticles combined with ultrasound-targeted MB destruction. Int J Nanomed 2017;12:7103–7119.
Trachootham D, Alexandre J, Huang P. Targeting cancer cells by ROS-mediated mechanisms: A radical therapeutic approach? Nat Rev Drug Discov 2009;8:579–591.
Tsai CH, Zhang JW, Liao YY, Liu HL. Real-time monitoring of focused ultrasound blood-brain barrier opening via subharmonic acoustic emission detection: Implementation of confocal dual-frequency piezoelectric transducers. Phys Med Biol 2016;61:2926–2946.
Tung YS, Vlachos F, Choi JJ, Deffieux T, Selert K, Konofagou EE. In vivo transcranial cavitation threshold detection during ultrasound-induced blood-brain barrier opening in mice. Phys Med Biol 2010;55:6141–6155.
Unga J, Hashida M. Ultrasound induced cancer immunotherapy. Adv Drug Deliv Rev 2014;72:144–153.
van Rooij T, Skachkov I, Beekers I, Lattwein KR, Voorneveld JD, Kokhuis TJ, Bera D, Luan Y, van der Steen AF, de Jong N, Kooiman K. Viability of endothelial cells after ultrasound-mediated sonoporation: Influence of targeting, oscillation, and displacement of microbubbles. J Control Release 2016;238:197–211.
van Wamel A, Kooiman K, Harteveld M, Emmer M, ten Cate FJ, Versluis M, de Jong N. Vibrating microbubbles poking individual cells: Drug transfer into cells via sonoporation. J Control Release 2006;112:149–155.
van Wamel A, Sontum PC, Healey A, Kvale S, Bush N, Bamber J, Davies CD. Acoustic Cluster Therapy (ACT) enhances the therapeutic efficacy of paclitaxel and Abraxane for treatment of human prostate adenocarcinoma in mice. J Control Release 2016;236:15–21.
Vignon F, Shi WT, Powers JE, Everbach EC, Liu JJ, Gao SJ, Xie F, Porter TR. Microbubble cavitation imaging. IEEE Trans Ultrason Ferroelectr Freq Control 2013;60:661–670.
VisualSonics. PN11691—Vevo MicroMarker Non-Targeted Contrast Agent Kit: Protocol and Information Booklet Rev. 1.4. Toronto: Author; 2016.
Wachsmuth J, Chopr R, Hynynen K. 2009 Feasibility of transient image-guided blood-spinal cord barrier disruption. AIP Conf Proc 2009;1113:256–259.
Wang JF, Zhao ZL, Shen SX, Zhang CX, Guo SC, Lu YK, Chen YM, Liao WJ, Liao YL, Bin JP. Selective depletion of tumor neovasculature by microbubble destruction with appropriate ultrasound pressure. Int J Cancer 2015;137:2478–2491.
Wang S, Olumolade OO, Sun T, Samiotaki G, Konofagou EE. Noninvasive, neuron-specific gene therapy can be facilitated by focused ultrasound and recombinant adeno-associated virus. Gene Ther 2015;22:104–110.
Wang SY, Wang CY, Unnikrishnan S, Klibanov AL, Hossack JA, Mauldin FW. Optical verification of microbubble response to acoustic radiation force in large vessels with in vivo results. Invest Radiol 2015;50:772–784.
Wang TY, Choe JW, Pu K, Devulapally R, Bachawal S, Machtaler S, Chowdhury SM, Luong R, Tian L, Khuri-Yakub B, Rao J, Paulmurugan R, Willmann JK. Ultrasound-guided delivery of microRNA loaded nanoparticles into cancer. J Control Release 2015;203:99–108.
Wang Y, Li Y, Yan K, Shen L, Yang W, Gong J, Ding K. Clinical study of ultrasound and microbubbles for enhancing chemotherapeutic sensitivity of malignant tumors in digestive system. Chin J Cancer Res 2018;30:553–563.
Weber-Adrian D, Thévenot E, O'Reilly MA, Oakden W, Akens MK, Ellens N, Markham-Coultes K, Burgess A, Finkelstein J, Yee AJ, Whyne CM, Foust KD, Kaspar BK, Stanisz GJ, Chopra R, Hynynen K, Aubert I. Gene delivery to the spinal cord using MRI-guided focused ultrasound. Gene Ther 2015;22:568–577.
Weber JS. Biomarkers for checkpoint inhibition. Am Soc Clin Oncol Educ Book 2017;37:205–209.
Wei YL, Shang N, Jin H, He Y, Pan YW, Xiao NN, Wei JL, Xiao SY, Chen LP, Liu JH. Penetration of different molecule sizes upon

ultrasound combined with microbubbles in a superficial tumour model. J Drug Target 2019;27:1068–1075.
Weiss HL, Selvaraj P, Okita K, Matsumoto Y, Voie A, Hoelscher T, Szeri AJ. Mechanical clot damage from cavitation during sonothrombolysis. J Acoust Soc Am 2013;133:3159–3175.
Weller GER, Villanueva FS, Klibanov AL, Wagner WR. Modulating targeted adhesion of an ultrasound contrast agent to dysfunctional endothelium. Ann Biomed Eng 2002;30:1012–1019.
Wiedemair W, Tukovic Z, Jasak H, Poulikakos D, Kurtcuoglu V. The breakup of intravascular microbubbles and its impact on the endothelium. Biomech Model Mechanobiol 2017;16:611–624.
Winterbourn CC. Reconciling the chemistry and biology of reactive oxygen species. Nat Chem Biol 2008;4:278–286.
Wu J. Theoretical study on shear stress generated by microstreaming surrounding contrast agents attached to living cells. Ultrasound Med Biol 2002;28:125–129.
Wu SY, Fix SM, Arena CB, Chen CC, Zheng W, Olumolade OO, Papadopoulou V, Novell A, Dayton PA, Konofagou EE. Focused ultrasound-facilitated brain drug delivery using optimized nanodroplets: Vaporization efficiency dictates large molecular delivery. Phys Med Biol 2018;63 035002.
Xhima K, Nabbouh F, Hynynen K, Aubert I, Tandon A. Noninvasive delivery of an α-synuclein gene silencing vector with magnetic resonance-guided focused ultrasound. Mov Disord 2018;33:1567–1579.
Xiao N, Liu J, Liao L, Sun J, Jin W, Shu X. Ultrasound combined with microbubbles increase the delivery of doxorubicin by reducing the interstitial fluid pressure. Ultrasound Q 2019;35:103–109.
Xing L, Shi Q, Zheng K, Shen M, Ma J, Li F, Liu Y, Lin L, Tu W, Duan Y, Du L. Ultrasound-mediated microbubble destruction (UMMD) facilitates the delivery of CA19-9 targeted and paclitaxel loaded mPEG-PLGA-PLL nanoparticles in pancreatic cancer. Theranostics 2016;6:1573–1587.
Xu R, O'Reilly MA. A spine-specific phased array for transvertebral ultrasound therapy: Design and simulation. IEEE Trans Biomed Eng 2020;67:256–267.
Yan F, Li L, Deng ZT, Jin QF, Chen JJ, Yang W, Yeh CK, Wu JR, Shandas R, Liu X, Zheng HR. Paclitaxel−liposome−microbubble complexes as ultrasound-triggered therapeutic drug delivery carriers. J Control Release 2013;166:246–255.
Yan P, Chen KJ, Wu J, Sun L, Sung HW, Weisel RD, Xie J, Li RK. The use of MMP2 antibody-conjugated cationic microbubble to target the ischemic myocardium, enhance Timp3 gene transfection and improve cardiac function. Biomaterials 2014;35:1063–1073.
Yang C, Du M, Yan F, Chen Z. Focused ultrasound improves NK-92 MI cells infiltration into tumors. Front Pharmacol 2019;10:326.
Yang J, Zhang XJ, Cai HJ, Chen ZK, Qian QF, Xue ES, Lin LW. Ultrasound-targeted microbubble destruction improved the antiangiogenic effect of Endostar in triple-negative breast carcinoma xenografts. J Cancer Res Clin Oncol 2019;145:1191–1200.
Yang Y, Zhang X, Ye D, Laforest R, Williamson J, Liu Y, Chen H. Cavitation dose painting for focused ultrasound-induced blood-brain barrier disruption. Sci Rep 2019;9:2840.
Yee C. Adoptive T cell therapy: Points to consider. Curr Opin Immunol 2018;51:197–203.
Yemane PT, Aslund A, Saeterbo KG, Bjorkoy A, Snipstad S, Van Wamel A, Berg S, Morch Y, Hansen R, Angelsen B, Davies CD. The effect of sonication on extravasation and distribution of nanoparticles and dextrans in tumor tissue imaged by multiphoton microscopy. Proc IEEE Int Ultrason Symp 2018; Available at: https://ieeexplore.ieee.org/document/8580082.
Yi S, Han G, Shang Y, Liu C, Cui D, Yu S, Liao B, Ao X, Li G, Li L. Microbubble-mediated ultrasound promotes accumulation of bone marrow mesenchymal stem cell to the prostate for treating chronic bacterial prostatitis in rats. Sci Rep 2016;6:19745.
Yu H, Chen S. A model to calculate microstreaming-shear stress generated by oscillating microbubbles on the cell membrane in sonoporation. Biomed Mater Eng 2014;24:861–868.
Yu H, Lin Z, Xu L, Liu D, Shen Y. Theoretical study of microbubble dynamics in sonoporation. Ultrasonics 2015;61:136–144.
Yu FTH, Chen X, Straub AC, Pacella JJ. The role of nitric oxide during sonoreperfusion of microvascular obstruction. Theranostics 2017;7:3527–3538.
Yuan H, Hu H, Sun J, Shi M, Yu H, Li C, Sun YU, Yang Z, Hoffman RM. Ultrasound microbubble delivery targeting intraplaque neovascularization inhibits atherosclerotic plaque in an APOE-deficient mouse model. In Vivo 2018;32:1025–1032.
Yuana Y, Jiang L, Lammertink BHA, Vader P, Deckers R, Bos C, Schiffelers RM, Moonen CT. Microbubbles-assisted ultrasound triggers the release of extracellular vesicles. Int J Mol Sci 2017;18 (8) pii: E1610.
Zafar A, Quadri SA, Farooqui M, Ortega-Gutierrez S, Hariri OR, Zulfiqar M, Ikram A, Khan MA, Suriya SS, Nunez-Gonzalez JR, Posse S, Mortazavi MM, Yonas H. MRI-guided high-intensity focused ultrasound as an emerging therapy for stroke: A review. J Neuroimaging 2019;29:5–13.
Zeghimi A, Escoffre JM, Bouakaz A. Role of endocytosis in sonoporation-mediated membrane permeabilization and uptake of small molecules: An electron microscopy study. Phys Biol 2015;12 066007.
Zhang M, Yu WZ, Shen XT, Xiang Q, Xu J, Yang JJ, Chen PP, Fan ZL, Xiao J, Zhao YZ, Lu CT. Advanced interfere treatment of diabetic cardiomyopathy rats by aFGF-loaded heparin-modified microbubbles and UTMD technique. Cardiovasc Drugs Ther 2016;30:247–261.
Zhang X, Owens GE, Cain CA, Gurm HS, Macoskey J, Xu Z. Histotripsy thrombolysis on retracted clots. Ultrasound Med Biol 2016;42:1903–1918.
Zhang L, Yin TH, Li B, Zheng RQ, Qiu C, Lam KS, Zhang Q, Shuai XT. Size-modulable nanoprobe for high-performance ultrasound imaging and drug delivery against cancer. ACS Nano 2018;12: 3449–3460.
Zhang LL, Zhang ZS, Negahban M, Jerusalem A. Molecular dynamics simulation of cell membrane pore sealing. Extreme Mech Lett 2019;27:83–93.
Zhao YZ, Tian XQ, Zhang M, Cai L, Ru A, Shen XT, Jiang X, Jin RR, Zheng L, Hawkins K, Charkrabarti S, Li XK, Lin Q, Yu WZ, Ge S, Lu CT, Wong HL. Functional and pathological improvements of the hearts in diabetes model by the combined therapy of bFGF-loaded nanoparticles with ultrasound-targeted microbubble destruction. J Control Release 2014;186:22–31.
Zhao YZ, Zhang M, Wong HL, Tian XQ, Zheng L, Yu XC, Tian FR, Mao KL, Fan ZL, Chen PP, Li XK, Lu CT. Prevent diabetic cardiomyopathy in diabetic rats by combined therapy of aFGF-loaded nanoparticles and ultrasound-targeted microbubble destruction technique. J Control Release 2016;223:11–21.
Zhou YF. Application of acoustic droplet vaporization in ultrasound therapy. J Ther Ultrasound 2015;3:20.
Zhou Y, Gu H, Xu Y, Li F, Kuang S, Wang Z, Zhou X, Ma H, Li P, Zheng Y, Ran H, Jian J, Zhao Y, Song W, Wang Q, Wang D. Targeted antiangiogenesis gene therapy using targeted cationic microbubbles conjugated with CD105 antibody compared with untargeted cationic and neutral microbubbles. Theranostics 2015;5:399–417.
Zhou H, Fang S, Kong R, Zhang W, Wu K, Xia R, Shang X, Zhu C. Effect of low frequency ultrasound plus fluorescent composite carrier in the diagnosis and treatment of methicillin-resistant *Staphylococcus aureus* biofilm infection of bone joint implant. Int J Clin Exp Med 2018;11:799–805.
Zhu HX, Cai XZ, Shi ZL, Hu B, Yan SG. Microbubble-mediated ultrasound enhances the lethal effect of gentamicin on planktonic *Escherichia coli*. Biomed Res Int 2014;2014 142168.
Zhu X, Guo J, He C, Geng H, Yu G, Li J, Zheng H, Ji X, Yan F. Ultrasound triggered image-guided drug delivery to inhibit vascular reconstruction via paclitaxel-loaded microbubbles. Sci Rep 2016;6:21683.